

Citation for published version:
Chen, Y, Wang, M, Liso, V, Samsatli, S, Samsatli, NJ, Jing, R, Chen, J, Li, N & Zhao, Y 2019, 'Parametric analysis and optimization for exergoeconomic performance of a combined system based on solid oxide fuel cell-gas turbine and supercritical carbon dioxide Brayton cycle', *Journal of Energy Conversion and Management*, vol. 186, pp. 66-81. https://doi.org/10.1016/j.enconman.2019.02.036

10.1016/j.enconman.2019.02.036

Publication date: 2019

Document Version Peer reviewed version

Link to publication

Publisher Rights CC BY-NC-ND

University of Bath

Alternative formats

If you require this document in an alternative format, please contact: openaccess@bath.ac.uk

General rights

Copyright and moral rights for the publications made accessible in the public portal are retained by the authors and/or other copyright owners and it is a condition of accessing publications that users recognise and abide by the legal requirements associated with these rights.

If you believe that this document breaches copyright please contact us providing details, and we will remove access to the work immediately and investigate your claim.

Download date: 09. Mar. 2023

Parametric analysis and optimization for exergoeconomic performance of a combined system based on solid oxide fuel cell-gas turbine and supercritical carbon dioxide Brayton cycle

Yunru Chen^a, Meng Wang^{a,b}, Vincenzo Liso^c, Sheila Samsatli^d, Nouri J Samsatli^e, Rui Jing^a, Jincan Chen^f, Ning Li^a, Yingru Zhao^{a,*}

^a College of Energy, Xiamen University, Xiamen 361005, China
 ^b School of Mechanical Engineering, Tongji University, Shanghai, 201804, China
 ^c Department of Energy Technology, Aalborg University, 9220 Aalborg East, Denmark
 ^d Department of Chemical Engineering, University of Bath, Claverton Down, Bath BA2 7AY,
 United Kingdom

^e Samsatli Solutions, Ventonlace, Flatwoods Crescent, Claverton Down, Bath BA2 7AH, United Kingdom

Abstract

Fuel cell-gas turbine hybrid system is a potential field of investigation. This study establishes a modeling and optimization framework for a novel hybrid system consisting of a solid oxide fuel cell, a gas turbine and a supercritical carbon dioxide Brayton cycle. Based on the proposed thermodynamical model, a parametric analysis is investigated to determine the impacts of several key parameters on the system exergoeconomic performance. Meanwhile, bi-objective optimization is conducted for maximizing the exergy efficiency and minimizing the levelized cost of electricity via the Epsilon-constraint approach. The Linear Programming Techniques for Multidimensional Analysis of Preference decision-making approach is further employed to select the Pareto optimum solution from Pareto frontiers. The results show that several extreme values for the exergy efficiency and the levelized cost of electricity exist in a series of sensitivity curves, respectively. The Pareto frontiers indicates that with the increase of the exergy efficiency, the levelized cost of electricity shows a moderately increasing trend at first and increases rapidly afterward. Overall, at the Pareto optimum solution, the combined system can achieve an optimal exergy efficiency and levelized cost of electricity by 68% and 0.0575 \$ kWh⁻¹, respectively.

Key words: solid oxide fuel cell-gas turbine; supercritical carbon dioxide Brayton cycle; parametric sensitivity analysis; exergoeconomic bi-objective; Pareto optimization

E-mail address: yrzhao@xmu.edu.cn (Y. Zhao).

^f Department of Physics, Xiamen University, Xiamen 361005, China

^{*} Corresponding author. Tel.: +86 592 5952781; Fax: +86 592 2188053

Nomenclature					
A	heat transfer area, m ⁻²	c	cathode		
c	capacitance rate, J (mol· K) ⁻¹	CC	combustion chamber		
CRF	capital recovery factor	com	compressor		
E	voltage, V	conc	ohmic voltage loss		
e_x	specific exergy, kJ kg ⁻¹	cold, hot	cold and hot streams		
\int_{F}^{x}	Faraday constant, C mol ⁻¹	DC	direct current		
ΔG^0	Gibbs free energy at the standard	e	electrolyte		
	pressure and temperature, J mol ⁻¹		0.000.0029.00		
h	specific enthalpy, J mol ⁻¹	eq	equipment		
i	current density, A m ⁻²	ex	exergetic		
i_0	exchange current density, A m ⁻²	f	fuel		
$i_{ m L}$	limiting current density, A m ⁻²	GT	gas turbine		
K , K_R , K_p	equilibrium constant	HEX	heat exchanger		
L	length, m	HTR	high temperature recuperator		
LHV	lower heating value, J mol ⁻¹	IHX	intermediate heat exchanger		
LCOE	levelized cost of the electricity, \$ kWh ⁻¹	inv	investment		
LMTD	logarithmic mean temperature difference, K	int	interconnect		
N	number of cells	LTR	low temperature recuperator		
n	molar flowrate, mol s ⁻¹	mc	maintenance		
n_{e}	number of electrons transferred	max	maximum		
p	pressure, MPa	min	minimum		
PR	pressure ratio	net	net power		
Q	heat transfer rate, kW	ohm	ohmic voltage loss		
S	active surface area, m ²	op	operation		
SR	split ratio	pp	pinch point temperature difference, K		
T	temperature, K	Pre	preheater		
TAC	total annual cost, \$	R	reforming reaction		
U	heat transfer coefficient, kW m ⁻² K ⁻¹	REC	recuperator		
$U_{ m f}$	fuel utilization factor	S	shifting reaction		
V	voltage, V	site	site development		
W	power, kW	sys	system		
Z	quantity of hydrogen participating	y	molar fraction		
	in the electrochemical reaction of SOFC				
Greek sym	Greek symbols		0 ambient (temperature, pressure)		
α	site development factor	Abbreviati	ons		
β	maintenance factor	CHP	combined heat and power		
η	efficiency	EPC	exergetic performance coefficient		
σ	electronic conductivity, S m ⁻¹	GE	gas expanders		

\mathcal{E}	effectiveness of exchanger	KC	Kalina cycle
τ	number of operational hours per	MED	multiple-effect distillation
	year		
Superscrip	ots	ORC	Organic Rankine cycle
ch	chemical	SCO ₂ BC	supercritical carbon dioxide
			Brayton cycle
ph	physical	SOFC	solid oxide fuel cell
Subscripts		TRCC	transcritical carbon dioxide cycle
a	anode		
AC	alternating current		
act	activation voltage loss		

1. Introduction

1

2 The global environmental problems caused by the massive use of fossil fuels have been 3 urgently addressed. The emergence of solid oxide fuel cells (SOFCs) and hybrid systems has attracted people's attention due to the high efficiency, modularity, and environmental 4 5 friendliness [1]. Due to the high temperature of exhaust, the SOFC can be integrated with 6 other power generation systems. The SOFC-gas turbine (SOFC-GT) is one of the popular 7 SOFC hybrid systems, which uses the GT to recycle the waste heat from the SOFC and improve the efficiency of the overall system. The first SOFC-GT combined system was 8 9 developed at the Fuel Cells Research Center, whose nominal power and efficiency were 220 kW and 57% [2], respectively. To date, a large number of researchers have been conducted on 10 11 modeling of the SOFC-GT system. Bao et al. [3] developed a hierarchical model library of 12 internal reforming (IR) SOFCs in general Process Modelling System (gPROMS) environment. The results showed that an obvious difference existed between the gas outlet temperature and 13 average solid temperature in distributed modeling. In addition, this research provide relatively 14 15 specific modeling methods in gPROMS platform. Sghaier et al.[4] established the energy and exergy balances of components in the pre-reforming SOFC-GT cycle, which was performed 16 17 using Engineering Equation Solver (EES) software. The results revealed that the increase of several parameters including the ambient temperature would reduce the overall efficiencies. In 18 addition, the system performance would decline with the utilization factor increasing. 19 El-Emam et al. [5] proposed an integrated gasification and SOFC system with a GT and a 20 21 steam cycle. The energy and exergy performance were performed based on two different kinds 22 of coal. The results showed that for the two scenarios, the first law efficiency was 38.1% and 36.7%, while the second law efficiency was 27% and 23.2%. Optimal integration strategies for a syngas fueled SOFC and GT hybrid were proposed by Zhao in [6]. The proposed model would evaluate the performance of combined systems whose output power were in 2000-2500 W m⁻². The results revealed that integrating a GT cycle could achieve a significant increase (19%) in system efficiency and increasing the isentropic efficiency of the GT or/and the compressors would lead to an obvious improvement in system efficiency. Pirkandi et al. presented four different kinds of combined systems with pressurized fuel cells in [7]. The findings indicated that the optimal electrical efficiency was 51% and the overall efficiency was 64%. What's more, the results revealed the cost of the SOFC-GT combined system was about 1692 \$ kW⁻¹. Shamoushaki et al. [8] presented thermodynamic, exergy, economic, and environment analysis of a SOFC-GT hybrid system. Multi-objective optimization of the system by NSGA-II algorithm was done. The results indicated that the optimum exergy efficiency was 57.7% and the cost was 0.0435 \$ s⁻¹. In addition, the most of entropy generation rate (32%) was related to combustion chamber.

However, the high temperature exhaust from the GT still contains a great quantity of available high-grade heat so that some researchers have studied how to make full use of this remaining energy. In recent years, many researches have been done to explore the coupled strategy of SOFC-GT with other bottoming cycle. Tan et al. [9] proposed an integrated SOFC-gas expanders (GE)-Kalina cycle (KC) system, indicating that the waste heat of the GE exhaust was utilized by the Kalina cycle to make an adding of 10.3% in system efficiency. In addition, the system energy efficiency reached 64.2% based on the fuel low heat value (LHV). Yan et al. [10] proposed a SOFC-GT-Organic Rankine cycle (ORC) combined system to

achieve the cascade energy utilization. In addition, a comparison between the different bottoming cycles were presented. The results showed that the ORC sub-system produced 12.6% more power output than that of the KC sub-system and the system overall efficiency could reach 67%. Zhang et al. [11] conducted a SOFC-GT-supercritical ORC (SORC) integrated system via parametric analysis, and the results showed that the energy efficiency and CHP efficiency of the whole system were 66.27% and 88.43%, respectively. Gholamian and Zare [12] compared the energy and exergy efficiencies of the SOFC-GT-ORC and SOFC-GT-KC systems, and the results showed that the performance of the combined system with the ORC bottoming cycle was superior to systems with the Kalina cycle. Besides, the second law efficiency of the two integrated systems could achieve 62.35% and 59.53%, respectively. Ehyaei and Rosen [13] investigated the optimization and thermo-economic analysis of a trigeneration system based on SOFC. The results showed that an increase of 8% in exergy efficiency and a decrease of 9.7% in cost when selected the optimal design parameters. In addition, the efficiency as well as the entropy rates would decline with the compressor pressure ratio increasing. Ebrahimi and Moradpoor proposed a cycle consisting of SOFC, micro GT (MGT), and ORC in [14]. A pinch analysis was done and for a practical case and the pinch point temperature difference in the steam generator was 10.24 °C. The results showed that fuel saving of about 45%, the energy and overall efficiency could reach 45% and 65%, respectively. Eveloy et.al integrated a bottoming ORC to SOFC-GT system to enhance power generation capacity and efficiency in [15]. This research compared the recovery capacity of six candidate ORC working fluids including toluene, benzene, R123, R245fa, cyclohexane, and cyclopentane. The results revealed that toluene would offer the best

45

46

47

48

49

50

51

52

53

54

55

56

57

58

59

60

61

62

63

64

65

performance among the six ORC fluids. In addition to the usage in power generation, the SOFC-GT can be employed in hybrid systems as well as combined heat and power (CHP) or combined cooling heating and power (CCHP). Akkaya et al. [16] evaluated a SOFC/GT CHP system based on the exergetic performance criterion and the simulation results indicated that a design based on the exergetic performance coefficient (EPC) criterion had considerable advantage according to the entropy-generation rate. Ahmadi et al. [17] analyzed the exergy efficiency and levelized cost of electricity (LCOE) of the hybrid system consisting of a SOFC, a GT, and a multiple-effect distillation (MED). Meanwhile genetic algorithm (GA) optimization was employed to increase the exergy efficiency from 57% up to 63.5% as well as decrease the LCOE from 0.0736 \$ kWh⁻¹ to 0.0643 \$ kWh⁻¹ simultaneously. Reyhani et.al [18] compared three kinds of combined cycles including SOFC-GT, SOFC-GT-Steam turbine (ST), and SOFC-GT-MED from the thermo-economic viewpoints. The results showed that the calculated improvement in the period of return of the three combined system were 9.88%, 6.78%, and 31.86%, respectively. The SOFC-GT combined with a transcritical CO₂ cycle (TRCC) was firstly proposed by Meng [19] who conducted the parametric analysis of the SOFC-GT-TRCC combined system and evaluated the systemic performance based on thermal efficiency. The results indicated that the system electrical could reach 69.26% under the given conditions and the compressor pressure ratio was benefits to the efficiency. Besides the ORC, Kalina cycles, and TRCC, selecting the supercritical carbon dioxide

67

68

69

70

71

72

73

74

75

76

77

78

79

80

81

82

83

84

85

86

87

88

Besides the ORC, Kalina cycles, and TRCC, selecting the supercritical carbon dioxide Brayton cycle (SCO₂BC) as the bottoming loop to recover the waste heat is an innovative and promising method. The SCO₂BC is another emerging efficient technology due to its advantages. Firstly, the SCO₂BC has a better environmental friendliness and safety because

carbon dioxide (CO₂) is a natural working fluid, which is innocuous and harmless. Therefore, the circulation system can cope with the leakage of the CO₂ working fluid, only requiring ventilation equipment. In addition, corrosion of turbine blades by droplet impingement can be completely avoided because the CO₂ working fluid will not undergo a phase change when it expands through the turbine in a supercritical state. Secondly, in comparison with superheated steam Rankine cycle, the SCO₂BC has a higher thermal efficiency with heat source temperatures above 820 K [20]. This is mainly because the inlet temperature of the turbine can be raised due to the fact that the CO₂ fluid is less corrosive than steam at the same temperature. Meanwhile, the compressor power consumption will reduce because of the incompressibility of CO₂ fluid near the critical point. Thirdly, since the minimum working pressure of the SCO₂BC is above the critical pressure, which is higher than the working pressure of the existing steam Rankine cycle and other Brayton cycles, the system structure is much more compact. Therefore, the volume flow of the working fluid is reduced, which makes the turbomachinery in the SCO₂BC considerably smaller than that in the steam Rankine cycle. Moreover, the cost of equipment can be reduced by modular production. In fact, the advantages of the SCO₂BC make it quite comfortable for a variety of applications such as nuclear reactors, solar energy, and waste heat recovery [21]. Al-Sulaiman and Atif compared the thermodynamic comparison of five SCO₂ Brayton cycles integrated with a solar power tower in [22]. The findings demonstrated that the recompression cycle reached the highest thermal efficiency as well as the net power generation. At June noontime for this cycle, the highest thermal efficiency was 52% and the system efficiency was 40%. Park et.al preformed the analysis of coal-fired power plant combined with SCO₂BC. The conclusions revealed that

89

90

91

92

93

94

95

96

97

98

99

100

101

102

103

104

105

106

107

108

109

the system efficiency was improved by 6.2-7.4% and the LCOE was reduced by 7.8-13.6% compared to the steam Rankine cycle. Ishiyama et.al [20] compared the fundamental performance of cycle efficiency and the construction cost for the ST, helium turbine and CO₂ turbine cycles in prototype fusion power reactor. The results demonstrated that at the heat source temperature of 480 °C, the cycle efficiency of the ST, helium turbine, and the SCO₂ cycles were 40%, 34%, and 42%, respectively. In addition, the component volumes of SCO₂ cycle were much smaller than those in ST cycle, thus resulting a lower construction cost. Hou et.al [23] proposed a hybrid system coupling SCO₂ recompression and regenerative cycle to recover the marine gas turbine exhaust heat. The multi-objective optimization was employed to optimized the output power, exergy efficiency, heat exchanger area per unit power output (APR) and the LCOE. The conclusions indicated that the system could effectively improve the full-load performance of the ship (12.38%). The system proposed by Sanchez et.al [24] was based on introducing bottoming closed cycle GT working with SCO₂ as opposed to open cycle hot air turbines used in conventional systems. The results showed that molten carbonate fuel cells (MCFCs)-SCO₂ could achieve 60% efficiency, which meant an increase of 10% with respect to the system using hot air turbines. Jokar et.al [25] concerned with the thermodynamic analysis and the optimization of a MCFC-SCO₂ Brayton hybrid system. Four objective including energy efficiency, power density, exergy destruction, and ecological function density were focused. During the multi-objective optimization, three scenarios were proposed. The results showed that a strong confliction between the objective functions existed and the maximum energy efficiency (66.76%) occurred in the third scenarios. For discussion of the common bottoming cycles, the characteristics of these cycles are presented and

111

112

113

114

115

116

117

118

119

120

121

122

123

124

125

126

127

128

129

130

131

summarized in Table 1.

In the literatures above, as a bottoming cycle, SCO₂BC has been integrated to kinds of power systems such as MCFC-GT, solar energy, nuclear reactor, and conventional power plant. However, the integration to SOFC-GT from the exergoeconomic viewpoint has not been investigated. In this paper, based on a heat-integrated configuration, a novel hybrid power generation system consisting of a SOFC, a GT, and a split-flow recompression SCO₂BC is investigated to explore the feasibility and the exergoeconomic performance of the SCO₂BC incorporated into SOFC-GT.

In addition, the existing combined systems aforementioned, whose topping loop is the SOFC-GT cycle, usually use the waste heat to preheat the reactants of the SOFC at first and then transfer heat to the downstream cycle. Different from them, the position of the heat exchanger in the proposed system is changed for a better match of the heat transfer temperature difference between the SOFC-GT and the SCO₂BC, the high-grade energy will be fully utilized as well.

The model is established and implemented in gPROMS 5.1.1 [26]. Since only the first law efficiency was applied as the criterion for evaluating the system performance in the most research works mentioned above, the impacts of several key parameters on the exergy and economic performance of the combined system are investigated. Meanwhile, the multi-objective exergoeconomic optimization has been conducted via the Epsilon-constraint (ε-constraint) approach in order to obtain the Pareto frontier based on two objective functions: the levelized cost of the electricity and the exergy efficiency. Finally, the optimum solution is selected from the Pareto frontier through linear programming techniques for

multi-dimensional analysis of preference (LINMAP), which is a typical decision-making method.

Table 1 The characteristics of three common bottoming cycles.

	Kalina Cycle	Organic Rankine Cyle	Supercritical CO ₂ Brayton Cycle
Heat source temperature	Low-medium temperature.	Low-medium temperature.	Medium-high temperature.
Working fluids	Ammonia-water mixture.	Organic fluid.	Carbon dioxide.
Advantages	Better coupling of temperatures between the working fluids and the source. Lower irreversibility in heat transfer process [27, 28].	Relatively compact system layout. Suitable working pressure, Especially suitable for the recovery and utilization of low-grade waste heat [29].	Good stability, Low corrosiveness, and environmental friendliness of working fluids [30]. Compact system layout [23]. High system efficiency [31].
Disadvantages	Additional shunt devices needed. High complexity of system, Poisonous and flammable working fluids [32].	Limited space for technics optimization. Environmental unfriendliness and toxicity of working fluids [33].	High requirements for equipment, especially compressors and turbines [34, 35]. Of most still in laboratory or demonstrations [21, 36].
Applications in coupling system	SOFC-GT [9, 12], Geothermal energy [32], Industrial waste heat [37, 38].	Solar energy [39], Geothermal energy [32], SOFC-GT [11, 14], Industrial waste heat [40, 41].	MCFC-GT [24, 25], Nuclear reactor[20], Industrial waste heat [42].

2. System's description and modeling

The layout of a SOFC-GT-SCO₂BC integrated system and the T-S diagram of the bottoming SCO₂BC are shown in Fig. 1 and Fig. 2, respectively. The upstream SOFC-GT sub-system and the downstream SCO₂BC with recompressing are integrated via thermal coupling to achieve better system performance.

2.1. System description

In Fig. 1, air goes through the compressor and preheater successively to obtain high pressure and temperature, and then enters the cathode side of the fuel cell. Similarly, fuel and water are mixed together and then fed into the anode side of the fuel cell to take part in the chemical

reactions with air after pressuring and heating. The energy produced by the electrochemical reaction in the fuel cell is used for power generation and heating reactants to the operating temperature. The unreacted fuel from the anode and the excess air from the cathode enter the combustion chamber for full combustion. The outlet stream of the combustion chamber is at high pressure and temperature. After an expansion process in turbine 1, the exhaust enters the heat exchanger (HEX) to provide heat energy for the bottoming cycle. After delivering heat in the HEX, the outlet stream enters preheater 1 to heat fuel and then splits into two streams to enter preheater 2 and preheater 3 for heating water and air, respectively, which ensures a feasible heat transfer temperature difference of the preheaters.



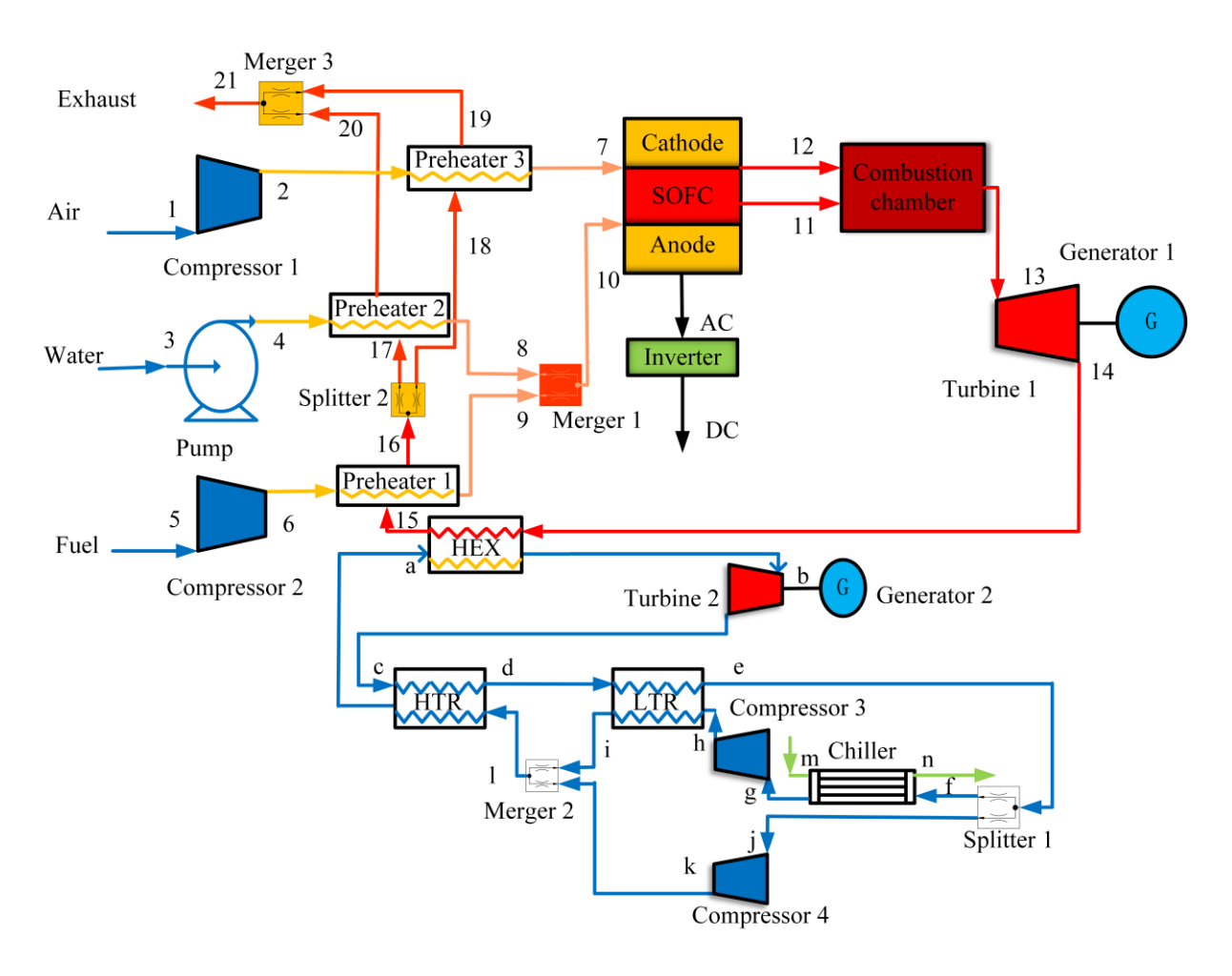


Fig. 1. The layout of a SOFC-GT- SCO₂BC combined system.

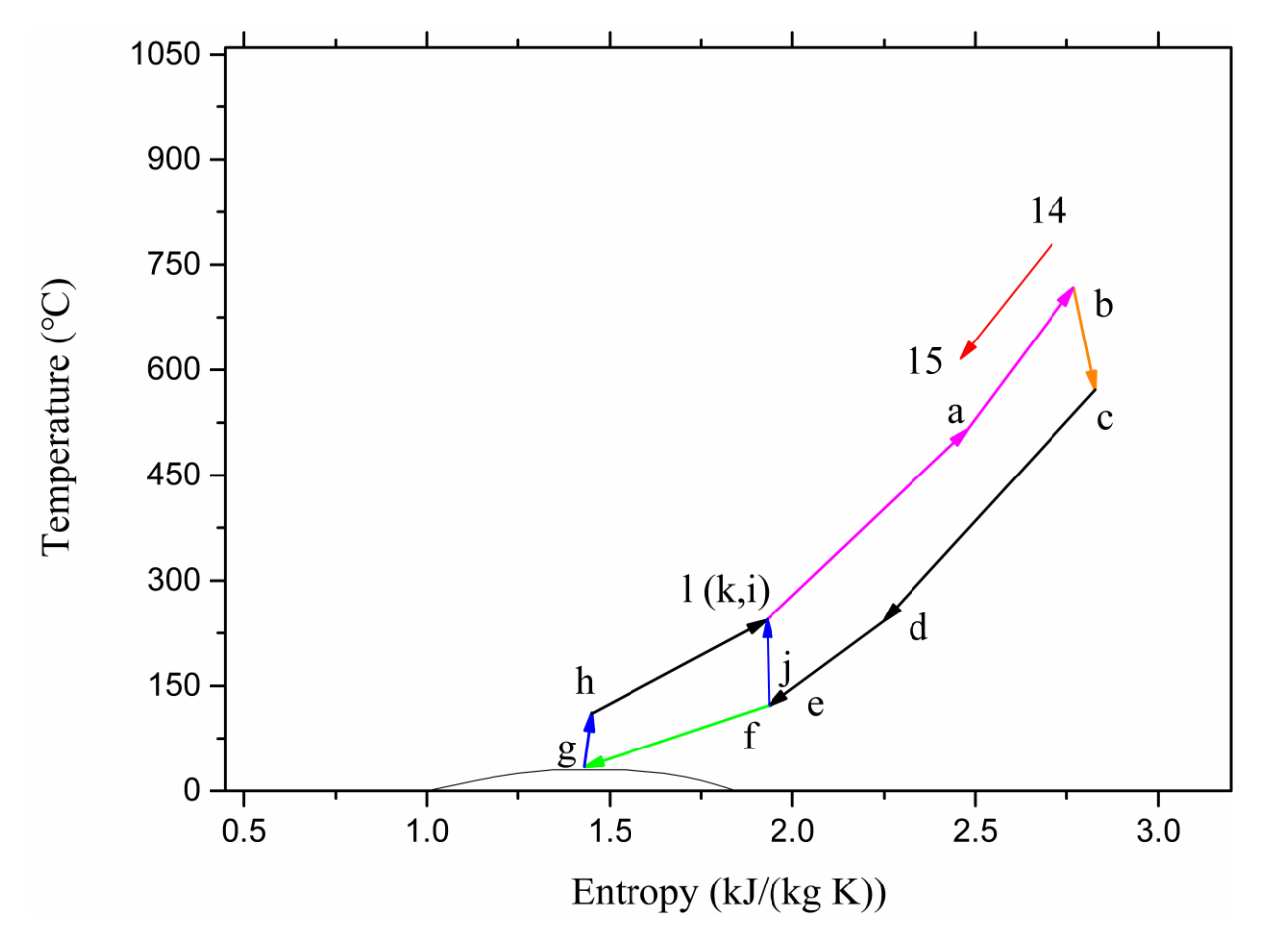


Fig. 2. The T-S diagram of the bottoming SCO₂BC.

In terms of the bottoming SCO₂BC, a recompression layout is adopted, which is one of the most extensively researched cycles in the literature [21]. There are two advantages to this layout. One is that the difference between the molar flowrates in the high and low pressure sides of the low temperature recuperator changes the heat capacities of the two streams (compared with other designs) such that the pinch point problem is alleviated. The other is that the size of the chiller is reduced as the heat load decreases. As shown in Fig. 1, the bottoming cycle is composed of one CO₂ turbine, two recuperators (a high temperature recuperator, HTR, and a low temperature recuperator, LTR), one chiller, and one primary heater. After expanding through the CO₂ turbine, the CO₂ fluid enters the HTR and LTR to release heat successively.

Next, the CO₂ working fluid is split into two flows, where one flow goes to the recycle compressor (compressor 4) directly and the other flow enters the chiller at first to reduce the temperature close to its critical value and then is compressed in the main compressor (compressor 3). After reheating in the LTR, it is mixed with another flow and goes through the HTR as well as the HEX. Then, the CO₂ working fluid is fed to the CO₂ turbine, producing power, and the bottoming cycle is completed.

2.2. Major specifications and modelling assumptions

- For the development of the hybrid system model, the following assumptions in this study are included for simplicity [10, 11, 19]:
- All the processes are considered steady state.

192

193

194

195

196

197

198

210

211

212

213

- The fuel is methane (CH₄), which is considered as ideal gas.
- Air comprises 79% nitrogen (N₂) and 21% oxygen (O₂).
- The anode and cathode pressures of the SOFC are assumed to be the same.
- Temperature for the air and fuel at the outlet channel of the cell is uniform and equal to the operating temperature of the cell.
- The gases in the combustion chamber are perfectly mixed.
- The pressure drops and heat loss in the components and connection tubes to the environment are negligible, except in the combustion chamber.
 - The leakage losses of the working fluid from the components as well as the connection tubes are neglected.

2.3. Main component modelling

In this section, the thermodynamic models of several main components including solid oxide

- fuel cell and heat exchangers are introduced in detail. The energy and exergy balance
- equations for each component and node are given in Appendix A. and B.

216 2.3.1. Solid oxide fuel cell

- 217 The internal reforming reactions are employed in this study and the reaction mechanisms in
- 218 the SOFC stack are therefore as follows:

$$CH_4 + H_2O \rightarrow CO + 3H_2$$
 (Reforming)

$$CO + H_2O \rightarrow CO_2 + H_2 \text{ (Shifting)}$$

221
$$H_2 + 0.5O_2 \rightarrow H_2O$$
 (Electrochemical)

- The equilibrium constants of reforming and shifting reactions are described according to
- 223 the partial pressures of reactants and products of these species and given by

$$K_{\rm R} = \frac{p_{\rm CO} \cdot p_{\rm H_2}^3}{p_{\rm CH_4} \cdot p_{\rm H_2O}} , \qquad (1)$$

$$K_{\rm S} = \frac{p_{\rm CO_2} \cdot p_{\rm H_2}}{p_{\rm CO} \cdot p_{\rm H_2O}} \quad . \tag{2}$$

They can be determined by the following temperature dependent correlation

$$\log K = AT^4 + BT^3 + CT^2 + DT + E,$$
 (3)

- where the constants A, B, C, D, and E for the reforming and shifting reactions are listed in
- 226 Table 4.
- The power output of the SOFC is calculated as

$$\dot{W}_{\text{SOFC}} = i \times N \times S \times V \,, \tag{4}$$

- where S is the active surface area, N is the cell number, i is the current density, which can be
- 229 expressed as

$$i = \frac{Zn_eF}{S \times N},\tag{5}$$

- and Z and n_e are the quantity of hydrogen (H₂) and the electron number taking part in the electrochemical reaction of the SOFC, respectively.
- The cell voltage is given by

$$V = E - V_{loss}, (6)$$

233 where E is the reversible cell voltage and calculated by the Nernst Equation [43]

$$E = -\frac{\Delta G^{0}}{n_{e}F} + \frac{RT}{n_{e}F} \ln(\frac{p_{H_{2}}\sqrt{p_{O_{2}}}}{p_{H_{2}O}}),$$
 (7)

- 234 ΔG^0 is the Gibbs free energy at the standard pressure and temperature, T is the operating
- 235 temperature of the SOFC, *R* is the universal gas constant, and *F* is Faraday constant.
- The voltage loss consists of three parts, which are the activation, ohmic, and concentration overvoltages, i.e.,
- 207 Concentration over voltages, i.e.,

239

240

241

242

$$V_{\text{loss}} = V_{\text{act}} + V_{\text{ohm}} + V_{\text{cont}}. \tag{8}$$

The above voltage loss can be calculated by following equations [6, 10]

$$V_{\text{act}} = \frac{2RT}{n_e F} \sinh^{-1}\left(\frac{i}{2i_0}\right),\tag{9}$$

$$V_{\text{con,a}} = -\frac{RT}{n_0 F} \ln(1 - \frac{i}{i_{1.0}}),$$
 (10)

$$V_{\text{con,c}} = -\frac{RT}{n_{\text{e}}F} \ln(1 - \frac{i}{i_{\text{L,c}}}),$$
 (11)

$$V_{\text{ohm}} = i \sum_{k} R_{k} = i \sum_{k} \frac{L_{k}}{\sigma_{k}} = i \left(\frac{L_{e}}{\sigma_{e}} + \frac{L_{a}}{\sigma_{a}} + \frac{L_{c}}{\sigma_{c}} + \frac{L_{\text{int}}}{\sigma_{\text{int}}} \right), \tag{12}$$

where i_0 is the exchange current density of the cell. $i_{L,a}$ and $i_{L,c}$ are the limiting current density of the anode and cathode, respectively, given by Ref. [44]. R_k is the resistance, L_k is the thickness, σ_k denotes the electronic conductivity of the anode, cathode, and interconnect and the ionic conductivity of the electrolyte. Detailed expression and constants are given in Ref.

243 [44].

248

252

253

254

255

256

257

258

259

260

The energy balance equation of the SOFC can be expressed as

$$\sum \dot{n}_{\rm in} h_{\rm in} = \sum \dot{n}_{\rm out} h_{\rm out} + \dot{W}_{\rm SOFC}. \tag{13}$$

245 The electrical efficiency and power output of the SOFC can be defined as

$$\eta_{\text{SOFC}} = \frac{\dot{W}_{\text{SOFC,AC}}}{\dot{n}_{\text{f}} L H V_{\text{f}}},\tag{14}$$

$$\dot{W}_{\text{SOFC,AC}} = \dot{W}_{\text{SOFC}} \eta_{\text{DC-AC}}, \tag{15}$$

where $\dot{n}_{\rm f}$ is the fuel molar flowrate, $LHV_{\rm f}$ is the lower heating value of the fuel, and $\eta_{\rm DC\text{-}AC}$ is the inverter efficiency.

2.3.2. Combustion chamber and gas turbine

The unreacted fuel from the SOFC enters the combustion chamber and burns completely. The energy balance equations given in Appendix A are written for calculating the flue gas temperature in the combustion chamber.

The turbomachinery in the topping cycle, which includes compressor 1, compressor 2, pump, and turbine 1, are all modeled. Turbine 1 provides the power requirement for the compressors and pump. The turbomachinery in the bottoming cycle includes compressor 3, compressor 4, and turbine 2, which meets the consumption power of these two compressors. The isentropic efficiency is introduced to estimate the performance of the compression and expansion processes. The enthalpy values of the exhaust at turbine 1 exit and CO₂ fluid at turbine 2 exit could be calculated, respectively, according to the inlet condition as well as the equations given in Appendix A.

2.3.3. Heat exchangers

261 For preheaters 1 and 3 in the topping cycle, the surface area of the heat transfer can be

262 computed as

$$A_{\text{pre}} = \frac{\dot{Q}_{\text{pre}}}{U_{\text{pre}} \times F_{\text{pre}} \times LMTD},$$
(16)

263 where U_{pre} , F_{pre} , and LMTD are the overall heat transfer coefficient, the logarithmic mean 264 temperature difference correction factor, and logarithmic mean temperature difference, 265 respectively.

The heat exchange process of preheater 2, which heats water from the liquid state to superheated steam, is separated into three sections: heating, evaporating, and superheating sections. The total heat transfer area is the sum of the areas of the three parts. The detailed calculation method can be seen in Ref. [45].

The printed circuit heat exchanger (PCHE) with high compactness and structural rigidity is employed as the heat exchangers (IHE, HTR, LTR, Chiller) in the bottoming SCO₂BC for reducing the volume of the heat exchangers. For the HTR and LTR heat exchangers, the effectiveness, which is defined as the ratio of the actual transfer rate of heat exchanged to the maximum heat transfer rate, is introduced. The effectiveness of the HTR and LTR can be expressed as:

$$\varepsilon_{\rm HTR} = \frac{h_{\rm c} - h_{\rm d}}{h_{\rm c} - h(p_{\rm d}, T_{\rm l})},\tag{17}$$

$$\varepsilon_{\rm LTR} = \frac{h_{\rm d} - h_{\rm e}}{h_{\rm d} - h(p_{\rm e}, T_{\rm h})},\tag{18}$$

where $h(p_d, T_l)$ is the enthalpy that the working fluid leaving the HTR would have if it were cooled to the temperature of state l (i.e. if the maximum amount of heat were transferred); $h(p_e, T_h)$ is similarly defined. In combination with the energy balance equations in Appendix A, the unknown parameters of the HTR and LTR can be calculated.

At present, the known cost calculation equation of the PCHE employed in the SCO₂BC is directly related to the conductance ($U \times A$) [46]. Consequently, the cost model of the heat exchanger simply assumes that the costs are proportional to ($U \times A$). For the sake of accurately illustrating the impacts of the changing carbon dioxide properties near the critical point, the heat exchangers in the bottoming SCO₂BC are discretized into sub-heat exchangers connected in series [47]. The state of the entrance and exit of each section can be determined according to the energy balance equation.

With regard to each sub-heat exchanger, the average capacitance rate of each flow can be
determined as

$$C = \frac{\dot{n}(h_{\rm in} - h_{\rm out})}{T_{\rm in} - T_{\rm out}}.$$
 (19)

The effectiveness of each sub-heat exchanger is expressed as [48]

280

281

282

283

284

285

286

289

$$\varepsilon_{\text{sub-HEX}} = \frac{\dot{Q}_{\text{in}}}{C_{\text{min}} (T_{\text{hot,in}} - T_{\text{cold,in}})},$$
(20)

wher $29\dot{Q}_{in}$ is the heat transfer rate in the sub-heat exchanger and C_{min} is the smaller of the capacitance rates of the hot and cold streams in the sub-exchanger. The Number of Transfer Units (*NTU*) of each sub-heat exchanger is dimensionless and can be expressed as

$$NTU = \begin{cases} \frac{\log(\frac{1-\varepsilon C_{R}}{1-\varepsilon})}{1-C_{R}}, & \text{if } C_{R} \neq 1\\ \frac{\varepsilon}{1-\varepsilon}, & \text{otherwise} \end{cases}$$
(21)

293 where C_R is the ratio of the minimum capacitance rate to the maximum capacitance rate of the 294 hot and cold streams in the sub-exchanger, i.e.,

$$C_{\rm R} = \frac{C_{\rm min}}{C_{\rm max}}.$$
 (22)

The conductance of each sub-heat exchanger is calculated by the *NTU* as well as minimum capacitance rate

$$(U \times A)_{i} = C_{\min} NTU_{i}. \tag{23}$$

The total conductance of the whole heat exchanger is calculated by accumulating the sub-heat exchanger conductance

$$U \times A = \sum_{i=1}^{N} (U \times A)_{i}.$$
 (24)

2.4. System thermal performance

299

300 The net output power of the SOFC-GT sub-system and the entire system can be calculated as

$$\dot{W}_{\text{SOFC-GT}} = \dot{W}_{\text{SOFC-AC}} + \dot{W}_{\text{turl}} - \dot{W}_{\text{com1}} - \dot{W}_{\text{com2}} - \dot{W}_{\text{pump}},$$
 (25)

$$\dot{W}_{\text{net}} = \dot{W}_{\text{SOFC-GT}} + \dot{W}_{\text{tur}2} - \dot{W}_{\text{com}3} - \dot{W}_{\text{com}4}$$
 (26)

The electrical efficiencies of the SOFC-GT stand-alone system and overall system can be expressed as

$$\eta_{\text{SOFC-GT}} = \frac{\dot{W}_{\text{SOFC-GT}}}{\dot{n}_{\text{f}} L H V_{\text{f}}}, \tag{27}$$

$$\eta_{\text{ele}} = \frac{\dot{W}_{\text{net}}}{\dot{n}_{\text{f}} L H V_{\text{f}}} \,. \tag{28}$$

The specific molar flow exergy concept is employed to assess the system's performance based on exergetic performance criteria. It only includes the physical and chemical exergy, neglecting the kinetic and potential exergy in this paper, i.e.,

$$e_{\mathbf{x}} = e_{\mathbf{x}}^{ph} + e_{\mathbf{x}}^{ch} \,, \tag{29}$$

where

$$e_{\mathbf{x}}^{ph} = (h - h_0) - T_0(s - s_0),$$
 (30)

$$e_{x}^{ch} = \sum_{k} y_{k} e_{x k}^{ch} + RT_{0} \sum_{k} y_{k} \ln y_{k}$$
(31)

- and y_k is the molar fraction of gas species 'k' in the gas mixture and $e_{x_k}^{ch}$ is the specific chemical exergy of component 'k'.
- For the sub-systems and whole system, the exergy efficiencies can be expressed as [12]

$$\eta_{\text{ex,SOFC}} = \frac{\dot{W}_{\text{SOFC,AC}}}{\dot{n}_{\text{f}} e_{\text{f}}^{ch}},\tag{32}$$

$$\eta_{\text{ex,SOFC-GT}} = \frac{\dot{W}_{\text{SOFC-GT}}}{\dot{n}_{\text{f}} e_{\text{f}}^{ch}},\tag{33}$$

$$\eta_{\rm ex} = \frac{\dot{W}_{\rm net}}{\dot{n}_{\rm f} e_{\rm f}^{ch}} \,. \tag{34}$$

- The equations for calculating the exergy values of the nodes marked in Fig. 1 are listed in
- 310 Appendix B.

311 **2.5. Economic analysis**

- 312 For the economic modeling of the proposed system, the total annual cost consists of
- 313 investment cost and operating and maintenance costs [17], ie.,

$$TAC = C_{\text{in v}} + C_{\text{mc}} + C_{\text{op}}. \tag{35}$$

- The total investment includes the cost of developments, land, and purchased-equipment,
- 315 which is calculated according to Table 2. The annual investment cost is determined by
- employing the capital recovery factor [17]

$$C_{\text{inv}} = CRF(C_{\text{eq}} + C_{\text{site}} + C_{\text{land}}), \qquad (36)$$

- where CRF is the capital recovery factor. It is a function of the interest rate, i, and the number
- of years, n, that the equipment have been in operation

$$CRF = \frac{i(1+i)^n}{(1+i)^n - 1}.$$
 (37)

In exergoeconomic analyses, the *CRF* usually has a range of 0.147-0.180 [7].

Furthermore, the site development costs and maintenance costs are estimated from percentiles of $C_{\rm eq}$ and $C_{\rm inv}$ as

$$C_{\text{site}} = \alpha C_{\text{eq}}$$
, (38)

$$C_{\rm mc} = \beta C_{\rm inv} \,. \tag{39}$$

where α is usually considered to be 20% and β is considered as 0.5% according to Ref.[17].

 C_{op} refers to the annual sum costs of fuel consumed in the SOFC, where the fuel unit cost is taken to be 0.005 \$ MJ⁻¹ according to Ref. [49]. The levelized cost of electricity (LCOE) can be defined as [23]

$$LCOE = \frac{TAC}{\tau \times \dot{W}_{\text{net}}},\tag{40}$$

where τ is the average annual operating time at nominal capacity and is taken to be 7500 h.

327

Table 2 The cost functions of the equipment in SOFC-GT sub-system and SCO₂BC.

Equipment	Cost function
Equipment	Cost function
SOFC-GT sub-system	
Gas turbine [50]	$\dot{W}_{\rm GT}(1318.5 - 98.328 \ln \dot{W}_{\rm GT})$
Compressor [50]	$91562(\frac{\dot{W}_{\rm com}}{445})^{0.67}$
Pump [50]	$705.48\dot{W}_{\text{pump}}^{0.71}(1+\frac{0.2}{1-\eta_{\text{pump}}})$
Fuel cell [17]	$S_{\text{SOFC}}(2.96T_{\text{SOFC}} - 1907)$
Electrical reformer [13, 17]	$10^5 (\frac{\dot{W}_{\rm SOFC,DC}}{500})^{0.7}$

Fuel cell auxiliaries [17]	$0.1C_{ m SOFC}$		
Combustion chamber [18]	$(\frac{46.08\dot{m}_{\rm CC}}{0.995 - \frac{P_{\rm GT}}{P_{\rm CC}}})(1 + \exp(0.018T_{\rm GT} - 26.4))$		
Preheater [18]	$8500 + 409(A_{\text{REC}}^{0.85})$		
SCO ₂ BC			
Recuperator [46]	$2500(U \times A)_{REC}$		
Heater [46]	$5000(U \times A)_{ m HEX}$		
CO ₂ -chiller [46]	$1700(U \times A)_{\text{Chiller}}$		
Turbomachinery+ Generator [46]	$600\dot{W}_{ m tur}$		

3. Methods of optimization and decision making

The combined SOFC-GT-SCO₂BC model is built in gPROMS platform and the properties of each state point in the system are calculated based on temperature, pressure, and composition by built-in Multiflash physical property functions. In order to explore the optimum performance of the overall system, the approaches of bi-objective optimization and decision making are employed and introduced in this section.

3.1. Objective functions

In this study, two objectives of maximizing exergy efficiency and minimizing LCOE have been considered to obtain the optimum values of design variables as well as provide a balance between the thermodynamic performance and the cost of the integrated system. In addition, the bi-objective trade-off optimization is employed to analyze the restrictive relationship between these two objectives, which are defined as follows.

The first objective function to be maximized is the exergy efficiency of the entire system,

343 i.e.,

$$Obj.Func.I = \eta_{ex} = \frac{\dot{W}_{net}}{\dot{n}_{f} \times e_{f}^{ch}} . \tag{41}$$

344 The second objective function to be minimized is the LCOE of the entire system, i.e.,

$$Obj.Func.II = LCOE_{sys} = \frac{TAC}{\tau \times W_{net}}.$$
 (42)

3.2. Constraints and design variables

To limit the results to a technically feasible range, a set of constraints are applied in this optimization. The limitations for each design variable and other constraints are given in Table 3. Noted that, the constraint of pinch point temperature difference in the SCO₂BC (10 K) is less stringent than that in the topping cycle (20 K) in the optimization according to Refs [51, 52]. Besides, the inlet temperature of the gas turbine (turbine 1) as well as the CO₂ turbine (turbine 2) should be under 1550 K and 1273 K due to the material temperature limit according to Refs [50, 53], respectively. The eight design variables considered in this optimization problem are the turbine 2 inlet pressure, split ratio of splitter 2, CO₂ molar flowrate, split ratio of splitter 1, fuel molar flowrate, operating temperature of the SOFC stack, utilization factor of the SOFC, and turbine 1 pressure ratio.

Table 3 Optimization constraints and ranges of design variables.

	Unit	Description	Range of design variables	
	— Unit	Description	From	То
Constraint				
T _{pp} [16, 51, 52]	K	Pinch point temperature difference	10.00/20.00	-
$T_{ m min}$	K	The minimum temperature of exhaust gas	373	-

T_{TIT1} [50]	K	The inlet temperature of turbine 1		1550
T _{TIT2} [53]	K	The inlet temperature of turbine 2		1273
Design variables				
P _b [21, 23, 52]	MPa	Values of turbine 2 inlet pressure	16.0	25.0
SR_{SOFC}	-	The split ratio of splitter 2	0.300	0.700
$\dot{N}_{{ m CO}_2}$	mol s ⁻¹	Values of CO ₂ molar flowrate	10.0	80.0
SR_{SCO2BC} [23, 52]	-	The split ratio of splitter 1	0.650	0.980
$\dot{N}_{ m f}$ [10]	mol s ⁻¹	Values of fuel molar flowrate	4.50	8.50
T_{SOFC} [6, 44, 54]	K	The operating temperature of SOFC	973	1273
$U_{\rm f}[8,12]$	-	The utilization factor of SOFC	0.700	0.900
PR [11, 55]	-	The pressure ratio of turbine 1	4.00	17.0

3.3. Pareto optimization

There exist several methods for solving the multi-objective optimization problem. The one applied in this study to identify the non-dominated optimum solution set is the ϵ -constraint method. The ϵ -constraint method works by converting all but one of the objective functions to inequality constraints and then solving multiple single-objective optimizations with different values for each of the constraints on the other objective functions. In this study, the proposed optimization model is developed in gPROMS platform. The nonlinear programming problem (NLP) is solved by sequence quadratic program (SQP) [56]. Then the Pareto frontier combining the results of all of these different optimizations is obtained by introducing ϵ

-constraint method [57]. All points on the Pareto frontier are optimum non-dominated solutions. An explanative flow chart of model solving procedure is presented in Fig. 3.

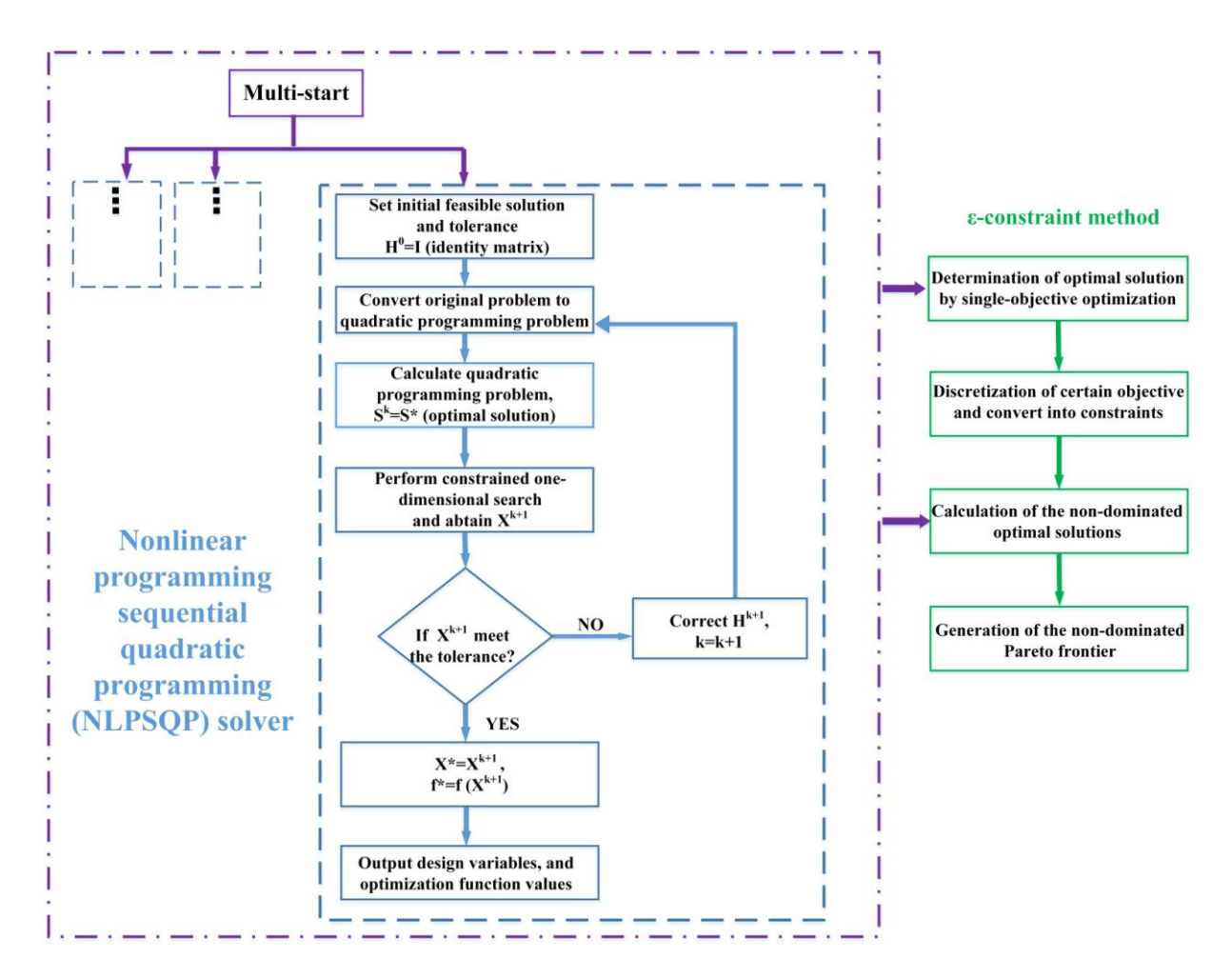


Fig. 3. Flow chart of multi-objective NLP model solving procedure.

3.4. Decision making

As the scales and dimensions of two objectives are different, both axes should be made dimensionless in order to determine the best applicable solution on the Pareto frontier. In this study, one of the most recognized non-dimensioned decision-making approaches named the LINMAP is employed to select the optimum point. The illustration of taking a bi-objective problem as an example is presented in Fig. 4. More detailed descriptions of the LINMAP

approach can be found in Refs. [58, 59].

In the LINMAP approach, the Euclidian distance ED_{i+} from each solution, i, on the Pareto frontier to the ideal point is expressed as

$$ED_{i+} = \sqrt{\sum_{j=1}^{n} (f_{ij} - f_{j}^{ideal})^{2}},$$
(43)

where f_j^{ideal} is the ideal solution of j_{th} objective in a single-objective optimization and f_{ij} is the value of the jth objective function in the ith solution. The solution with shortest Euclidian distance from ideal point is then selected as a final prior optimum solution and i_{final} is [60]

$$i_{\text{final}} = i \in \min(ED_{i+}). \tag{44}$$

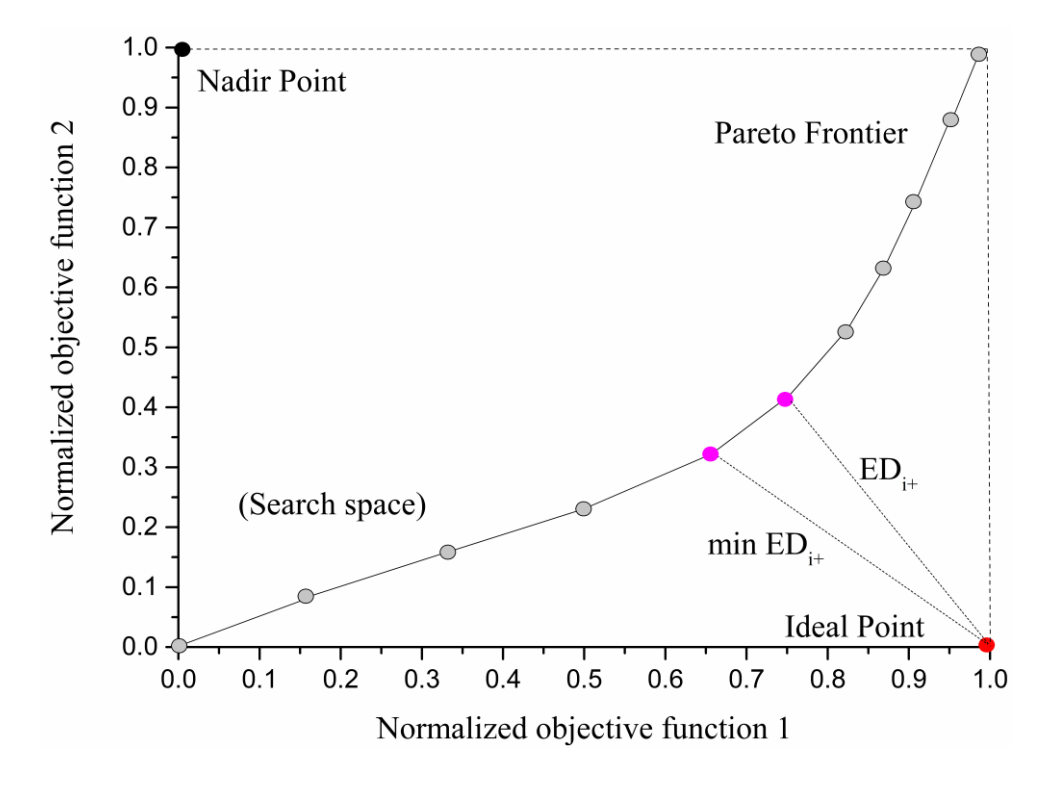


Fig. 4. Illustration of non-dominated and LINMAP decision-making approach.

4. Results and discussion

This section presents the results of the exergoeconomic performance and optimization of the proposed system. The impacts of six key parameters on system performance are paid attention.

The second law efficiency and the LCOE of the overall system are selected as the objective functions in the bi-objective optimization.

4.1. Model validation

In order to validate the model, the simulation results of the SOFC-GT sub-system are compared with the simulation data reported in Ref. [10] for the same input parameters. In terms of the bottoming split-flow recompression SCO₂BC, the parameters of this model are set according to the schematic diagram and data of the Argonne recompression split-flow SCO₂BC from Argonne National Laboratory [61]. The comparison between the simulation results and the experimental data are investigated. The input parameters adopted in the combined system are shown in Table 4 and the comparison results are listed in Table 5 in detail. Table 5 indicates a good agreement between the simulation results in this work and those in relevant references. Therefore, the process simulation of the present combined system is quite precise.

Table 4 Parameters setting in this simulation.

Term	Unit	Value
Ambient temperature [11]	K	298
Ambient pressure [23]	MPa	0.101
Fuel compressor isentropic efficiency [10]	%	82.0
Air compressor isentropic efficiency [10]	%	82.0
Pump efficiency [19]	%	80.0
Gas turbine isentropic efficiency [19]	%	75.0
Steam-to-carbon ratio [19]	-	2.20
Area of a cell [19]	cm^2	220
Cells number [19]	-	50,000
DC-AC inverter efficiency [14, 54]	%	95.0
Combustion chamber efficiency [19]	%	95.0
CO ₂ -turbine isentropic efficiency [52]	%	80.0
CO ₂ -compressor isentropic efficiency [52]	%	85.0
Pinch point temperature difference [10]	K	20.00
The recuperator effectiveness [14, 24]	%	92.0

CO ₂ -turbine outlet pressure [23]	MPa	7.40
Condenser inlet/outlet temperature [23]	K	298/320
$A_{\rm R}; A_{\rm S} [9, 17]$	-	-2.63×10 ⁻¹¹ ; 5.47×10 ⁻¹²
$B_{\rm R}; B_{\rm S}[9, 17]$	-	1.24×10 ⁻⁷ ; -2.57×10 ⁻⁸
$C_{\rm R}$; $C_{\rm S}$ [9, 17]	-	-2.25×10 ⁻⁴ ; 4.63×10 ⁻⁵
$D_{\rm R}; D_{\rm S}[9, 17]$	-	1.95×10 ⁻¹ ; -3.91×10 ⁻²
$E_{\rm R}; E_{\rm S} [9, 17]$	-	-6.61×10; 1.32×10

Table 5 Comparison of the simulation results of the SOFC-GT sub-system and the SCO₂BC with the data obtained from references.

Parameter	Yan	Sienicki	Present	Difference
Farameter	[10]	[61]	work	(%)
Cell operating voltage (V)	0.614	-	0.626	2.11
SOFC (DC) power output (kW)	3126	-	3124	0.06
GT power output (kW)	1642	-	1698	3.41
SOFC electrical efficiency (%)	48.80	-	48.82	0.04
GT outlet temperature (K)	-	635.3	637.8	0.39
First law efficiency (%)	-	39.10	38.70	1.02

4.2. Sensitivity analysis

412 Several key parameters like the fuel flowrate, fuel utilization factor of the SOFC stack, etc.,

significantly influence the performance of the entire system. Their impacts on performance of

the integrated system are investigated in the following sensitivity analysis.

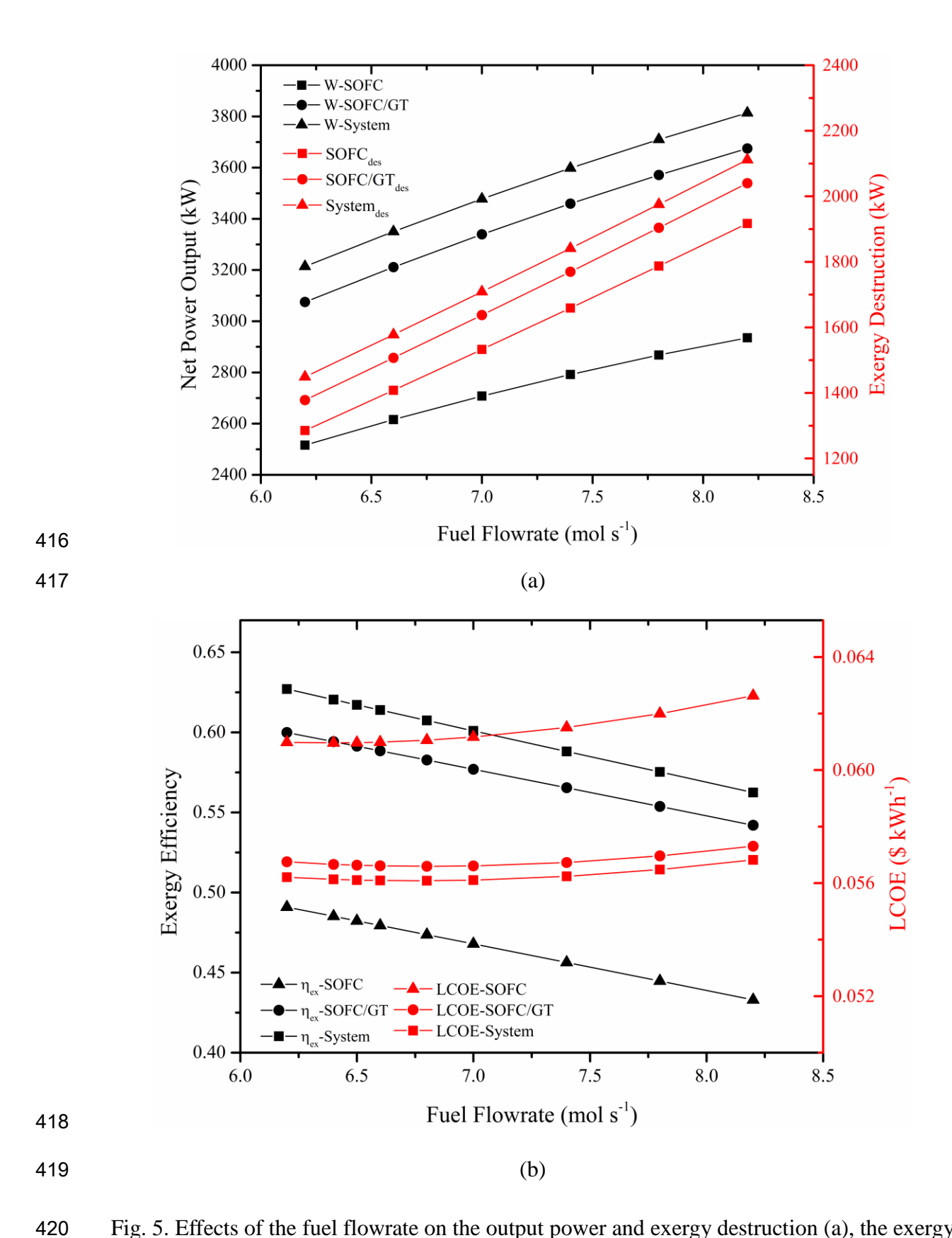


Fig. 5. Effects of the fuel flowrate on the output power and exergy destruction (a), the exergy efficiency and LCOE (b) for the combined system.

The variations of the output power and exergy destruction of the SOFC, SOFC-GT stand-alone system, and entire system with fuel flowrate are shown in Fig. 5(a). According to Fig. 5(a), higher power output as well as the exergy destruction of the integrated system are obtained compared with the SOFC-GT stand-alone system. As expected, it can be seen that higher fuel flowrates increase the output power and the exergy destruction of the system. Fig. 5(b) shows the effects of the fuel flowrate on the exergy efficiencies and LCOE of the SOFC, SOFC-GT sub-system, and entire system. The combined system achieves higher exergy efficiency and lower LOCE compared to the SOFC-GT stand-alone system. It is obvious that the exergy efficiencies of the SOFC, SOFC-GT sub-system, and entire system will decrease along with the fuel flowrate increasing, which is in accordance with the results in Refs. [11, 14]. This is mainly because although the output power increases, the increment of fuel flowrate is larger, thus resulting in the decrease of exergy efficiencies. Besides, when the fuel flowrate is 6.4 mol s⁻¹, the SOFC (on its own) will attain its minimum value of the LCOE. The optimum fuel flowrates for the LCOE of the SOFC-GT sub-system and combined system are both 6.8 mol s⁻¹. The reason is that the power output will ascend with the increase in fuel flowrate, as shown in Fig. 5(a). Meanwhile, the investment of equipment purchases in the SOFC-GT sub-system and the fuel cost will increase. The combined effect of the two factors is that the LCOE tends to decrease at first and then increase.

423

424

425

426

427

428

429

430

431

432

433

434

435

436

437

438

439

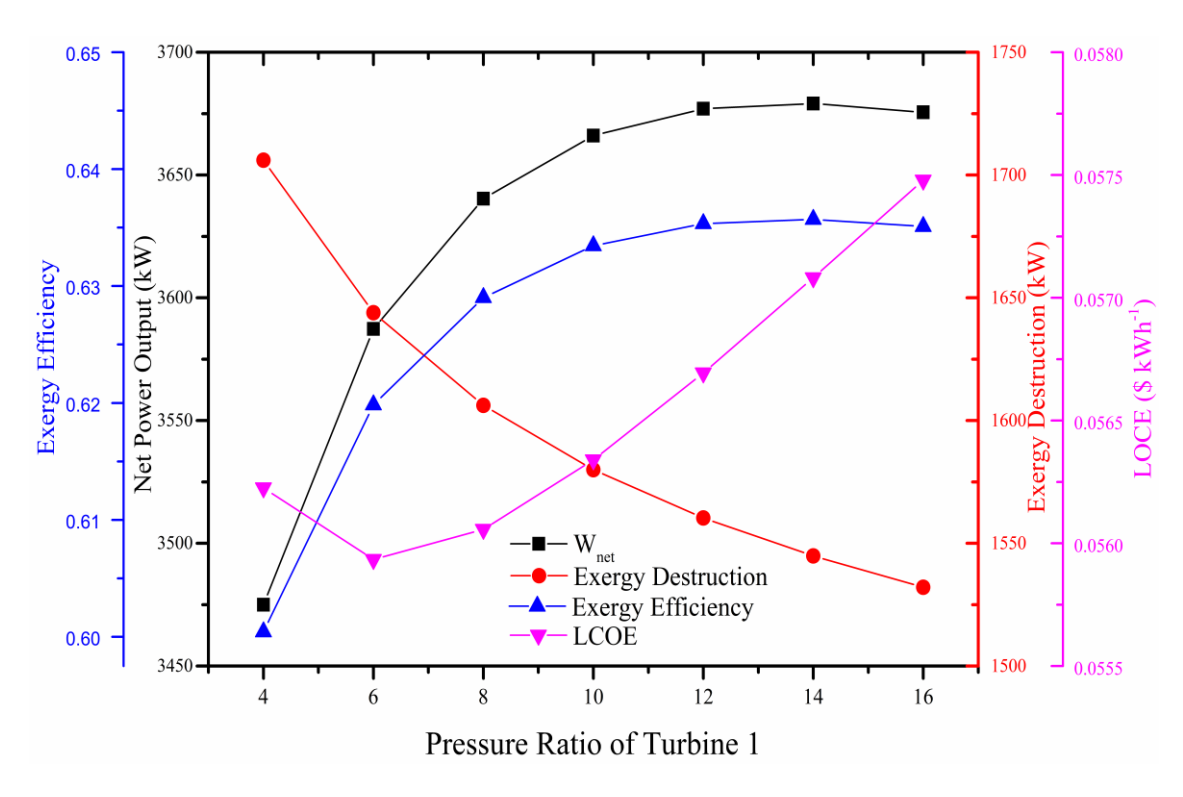


Fig. 6. Effects of the pressure ratio of turbine 1 on different parameters for the combined system.

Fig. 6 illustrates how the pressure ratio of turbine 1 influences the system-wide exergoeconomic performance. Note that while the pressure ratio increases, the output power and the exergy efficiency of the integrated system will rise quickly at first and then more gently. Finally, the trend shows a slight decline. The result indicates that the benefit for improving the exergy efficiency by increasing pressure ratio will become smaller with the increase of the pressure ratio. When the pressure ratio is 14, the output power and exergy efficiency have the maximums. This is because the higher operating pressure in the SOFC stack will cause a higher cell voltage, resulting in a larger power output of the SOFC. Meanwhile, more pressure drop through turbine 1 will produce more power output, which in turn results in a decline in the outlet temperature of turbine 1 as well as the power supplied to

the bottoming SCO₂BC accordingly. What's more, with the pressure ratio increases, the increment of output power for SOFC-GT is smaller than the decrement of that for SCO₂BC. Meanwhile, due to the output power of SOFC stack increases, the quantity of heat for preheating the entrance reactants decreases, the SOFC inlet temperature (outlet temperature of preheaters) increases accordingly, thereby decreasing the temperature difference as well as the exergy destruction in the preheaters. The large drop in the exergy destruction of the preheaters is the main cause of the monotonous decline in system exergy destruction. In addition, it is clear that by increasing the pressure ratio, the LCOE of the entire system will decrease at first and then increase, and there exists a lowest LCOE when pressure ratio is 6. This is mainly because the larger pressure ratio will result in higher purchase costs of equipment including gas turbine and compressors. Consequently, there should be a balance between the exergy efficiency and the LCOE of the combined system.

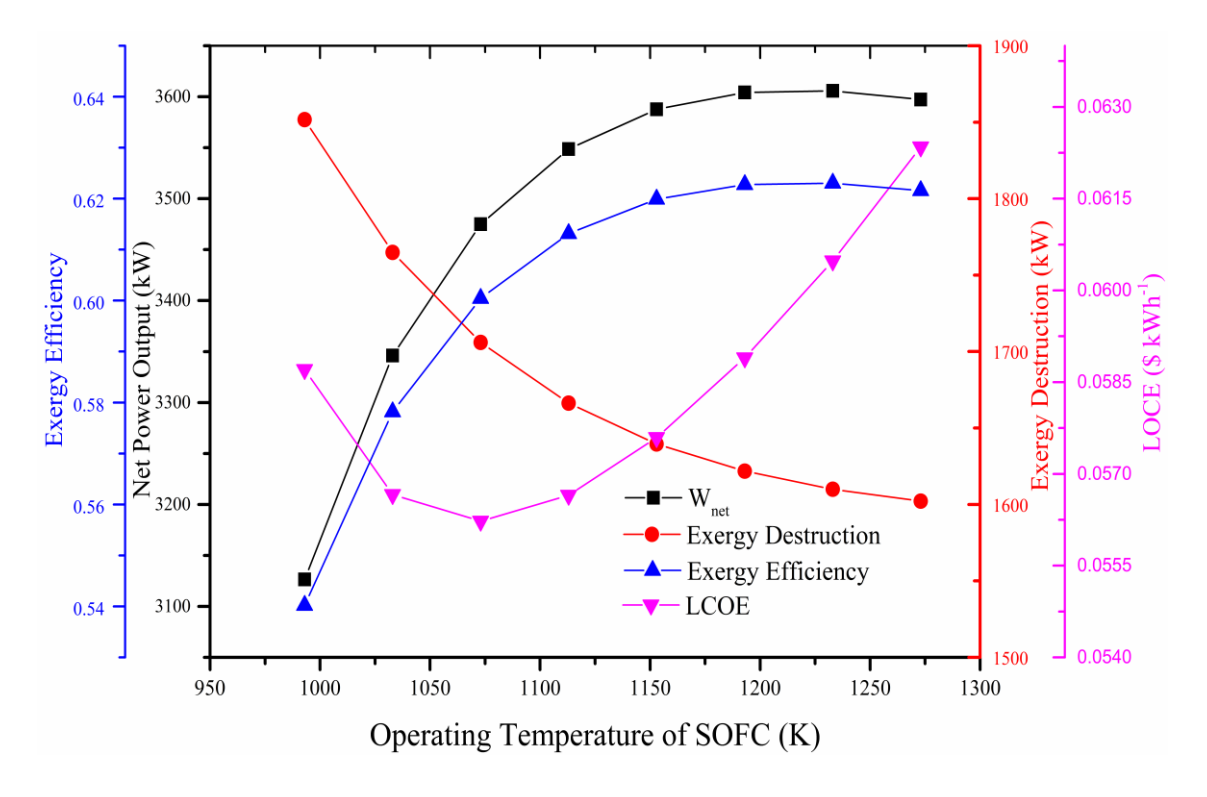


Fig. 7. Effects of the SOFC stack operating temperature on different parameters for the

471

472

473

474

475

476

477

478

479

480

481

482

483

484

485

486

The variations of the four important parameters of the combined system with the SOFC stack operating temperature are presented in Fig. 7. Note that the output power and the exergy efficiency will have peak values when the operating temperature is 1233 K. This is mainly because with the operating temperature increasing, the cell voltage will rise at first and then decline, resulting in the same variation trend of the SOFC power output with the constant current density. The same trend can be found in Ref. [12]. Although the power output of the gas turbine and CO₂ turbine will keep increasing due to the higher inlet temperature, the total output power and exergy efficiency will pass through their maximums. Referring to Fig. 7, the exergy destruction keeps monotonously decreasing with operating temperature increasing, which mainly results from the declines in exergy destruction of SOFC stack, combustion, and preheater 3. In addition, Fig. 7 indicates that when the operating temperature is 1073 K, the LCOE will achieve its minimum value. This is because, although the output power of the hybrid system will increase with the increase of the operating temperature at first, the purchase cost of the equipment mainly including the SOFC stack and turbines will also increase and seem more intense, which results in an optimal LCOE. As a result, the tradeoff between the exergy efficiency and the LCOE should be considered.

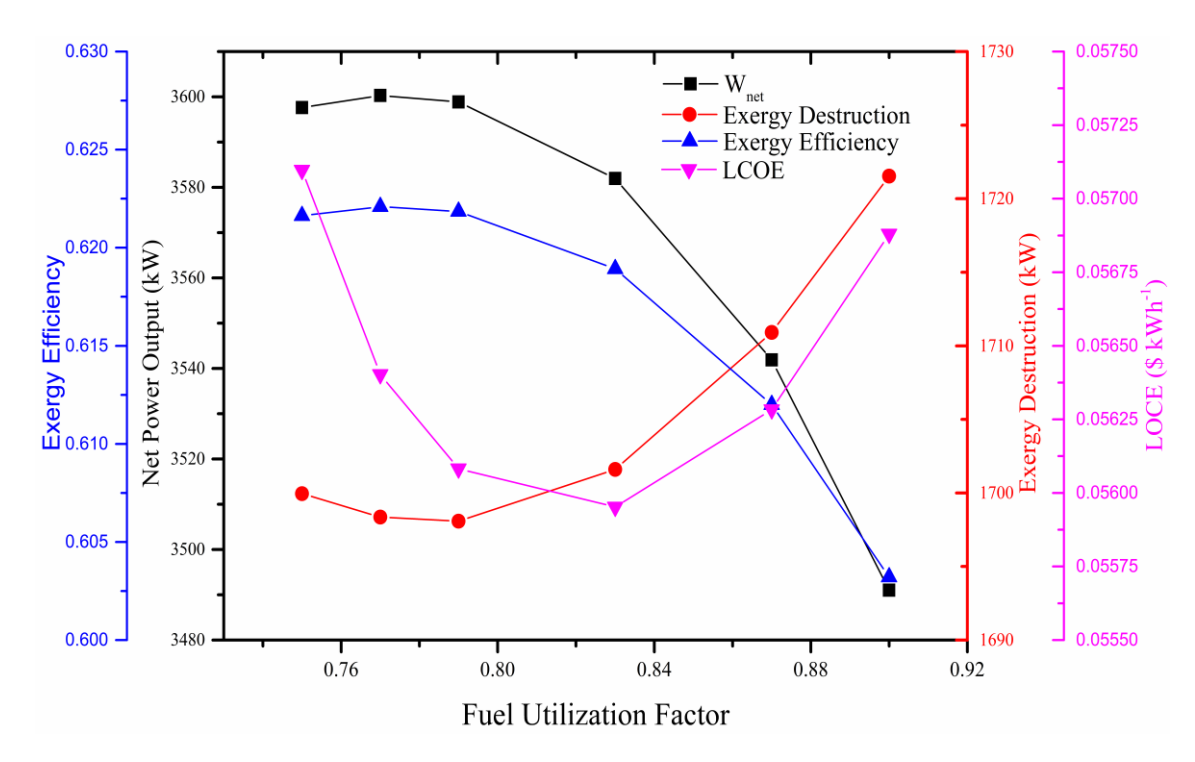


Fig. 8. Effects of the fuel utilization factor ($U_{\rm f}$) on different parameters for the combined system.

Fig. 8 is plotted to investigate how the fuel utilization factor (U_f) influences the exergoeconomic performance of the combined system. It is observed that with the increase of U_f , the output power and exergy efficiency will rise slightly at first and then reduce sharply in the last region. When the utilization factor is 0.77, the exergy efficiency will attain their maximum values. This is because that the increasing utilization factor means more hydrogen consumed in the SOFC stack, which simultaneously increases the current density and decreases the voltage due to the internal irreversibility [4]. In addition, the outlet temperature of the combustion chamber will become lower as the available hydrogen is reduced, which further results in a decrease in the power supplied to the gas turbine and the SCO₂BC. It is worth noting that the results in Refs. [9, 16] also suggested that the exergy efficiency of the SOFC-GT sub-system would go through a maximum via the variation of U_f . What's more, the

exergy destruction of the combined system has the minimum value which is also optimal when the U_f is 0.79. The monotonous decreasing exergy destruction in the SCO₂BC (mainly in the HTR and LTR) makes the decline at the beginning, but with the increasing U_f , the increase of exergy destruction in the SOFC-GT stand-alone system becomes dominant. Regarding the LCOE of the entire system, at low values of U_f , the increase of U_f results in the increase of the LCOE. On the contrary, at high values of U_f , it is found that the LCOE decreases with the increase of U_f . The minimum LCOE will be achieved when U_f is 0.83. The main reason is that with the increase of U_f , the energy for preheating in the SOFC stack will rise and result in a reduction of the heat load and heat transfer area of the preheaters, which in turn means a lower investment cost for the preheaters. In addition, U_f indirectly influences the operating temperatures of the gas turbine, CO_2 turbine, and combustion chamber sections, thereby reducing the corresponding investment. However, when U_f is larger than 0.83, the LCOE is found to increase with the increase of U_f . This is because the decreasing power output is dominant in this condition.

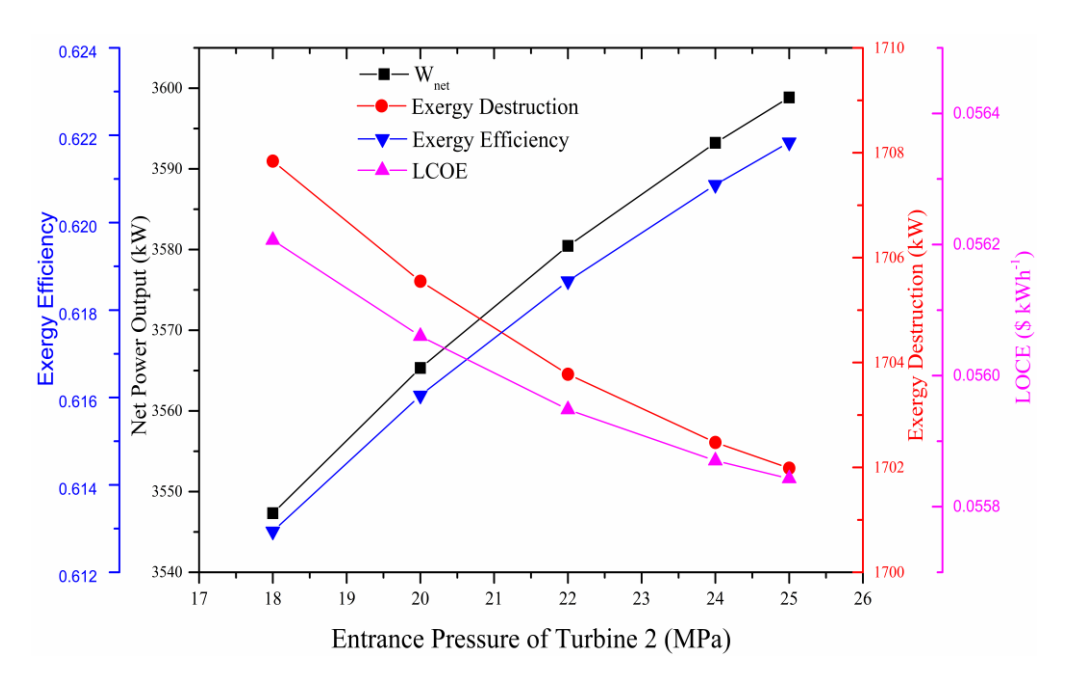


Fig. 9. Effects of turbine 2 entrance pressure on different parameters for the combined system.

The impacts of turbine 2 entrance pressure on the exergoeconomic performance of the entire cycles are illustrated in Fig. 9. It is clearly seen from this figure that the output power and the exergy efficiency will increase monotonically with increasing entrance pressure. On the other hand, the exergy destruction and LCOE will decline with the increase of the entrance pressure. The main reason is that turbine 2 will produce more power for a larger entrance pressure when the cooling pressure is constant. Although larger operating pressures will make the investment increase, the increase of the power output takes the dominant position, which makes a monotonic decrease of the LCOE. Although increasing the entrance pressure will improve the entire systemic exergoeconomic performance, the maximum entrance pressure employed in the present study is 25 MPa due to the maximum pressure limit of the equipment material. In addition, it can be clearly seen that the turbine 2 entrance pressure has a smaller effect on the entire system than the above parameters, as this parameter only influences the SOFC-GT sub-system slightly.

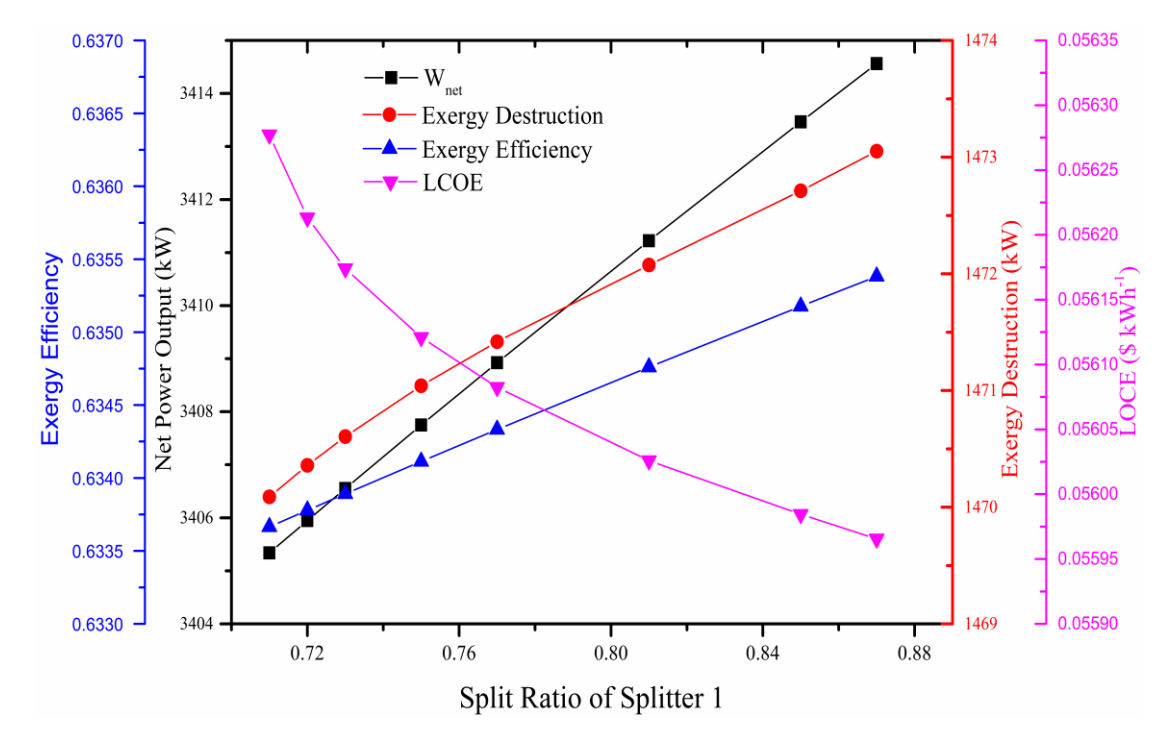


Fig. 10. Effects of the split ratio of the SCO₂BC on different parameters for the combined system.

Fig. 10 reveals the influence of the split ratio of the SCO₂BC on the combined system exergoeconomic performance. The split-flow recompression configuration is employed in the SCO₂BC since it is considered to be one of the most feasible cycles to solve the pinch problem of the internal recuperator. Furthermore, there exists a low limit of the split ratio, because the deterioration phenomenon will occur when the split ratio is smaller than a certain value [52]. It is noteworthy that, as the split ratio increases, the output power, exergy destruction, and the exergy efficiency will rise monotonically. This is mainly due to the fact that the total consumption power of the compressors in the SCO₂BC will reduce with the increasing split ratio. In addition, the split ratio makes little impacts in the topping cycle but increases exergy destruction in the HTR due to the bigger temperature difference. Although the increment in

exergy destruction of the combined system is small, the results indicates that the minimum exergy destruction does not always give the best system performance in the proposed system. Moreover, the LCOE will decrease with the increasing split ratio. The reason includes two aspects. One is that the net power output will keep increasing. The other is that the investment (mainly the investment of the internal recuperators) will decline, resulting from the decrease in the heat transfer area of the LTR with the increasing split ratio. Consequently, the split ratio can be improved properly when the pinch point temperature difference is in a reasonable range.

4.3. Pareto frontier and optimum solution

The Pareto frontier determined by the ε-constraint method is depicted in Fig. 11. The point labeled A in this figure shows the lowest LCOE (0.05452 \$ kWh⁻¹) as well as the lowest exergy efficiency (64.7%), which is effectively a single-objective optimization minimizing objective 1. Point C indicates that 69.2% is the maximum exergy efficiency of the proposed combined system with the worst economic performance, whose LCOE is 0.0633 \$ kWh⁻¹. It is the equivalent of a single-objective optimization of objective 2. All of the points in-between represent the minimization of objective 1 with progressively more stringent constraints on objective 2, to make it increase.

It is obvious that improving the entire system exergy efficiency is at the cost of raising the LCOE. In addition, the LCOE can be seen to increase moderately at first, with the increasing exergy efficiency, and then to increase more rapidly. To provide a good relation between the exergy efficiency and the LCOE, the fitted curve derived from Pareto frontier is obtained via polynomial fitting. The expression is as follows:

$$LCOE = 13957 \eta_{\text{ex}}^4 - 37246 \eta_{\text{ex}}^3 + 37269 \eta_{\text{ex}}^2 - 16573 \eta_{\text{ex}} + 2763.4,$$
(45)

571 where $64.7\% < \eta_{\text{ex}} < 69.2\%$, $R^2 = 0.9845$.

It is further seen from Fig. 11 that the Pareto optimum solution selected by the LINMAP method is point B, which has the shortest distance from the ideal point. Point B is with the exergy efficiency of 68.14% and the LCOE of 0.05751 \$ kWh⁻¹. The values of design variables and the corresponding performance optimization results for points A-C are listed in detail in Table 6. Referring to Table 6, the ultimate energy efficiency of the combined system is 71.55%, which is larger than those of the SOFC-GT-SORC integrated system (66.27%) in Ref [11], the SOFC-GT-KC system (64.2%) in Ref [9], and the SOFC-GT-TCO₂ integrated system (69.26%) in Ref [19]. Besides, the increment of exergy efficiency by integrated an ORC to SOFC-GT system is 10.33% according to Ref [12], which is lower than the increase (11.72% at point A) in the present study. In addition, the minimum LCOE (0.05452 \$ kWh⁻¹) in the proposed system is a little lower than that of a triple cycle based on a solid oxide fuel cell and gas and steam cycles (0.055 \$ kWh⁻¹) in Ref [13].

It is found from Table 6 that the maximum value of the system net output power as well as the destruction are obtained when the LCOE is lowest. What's more, with the increase of the system exergy efficiency, the benefit of combing the SCO₂BC to the SOFC-GT stand-alone system reduces. In addition, the values of the temperature, pressure, and molar flowrate of all nodes marked in Fig. 1 are listed in Appendix C in order to show the specific characteristics of most of the components of the proposed system in detail, when it operates at the optimum condition.

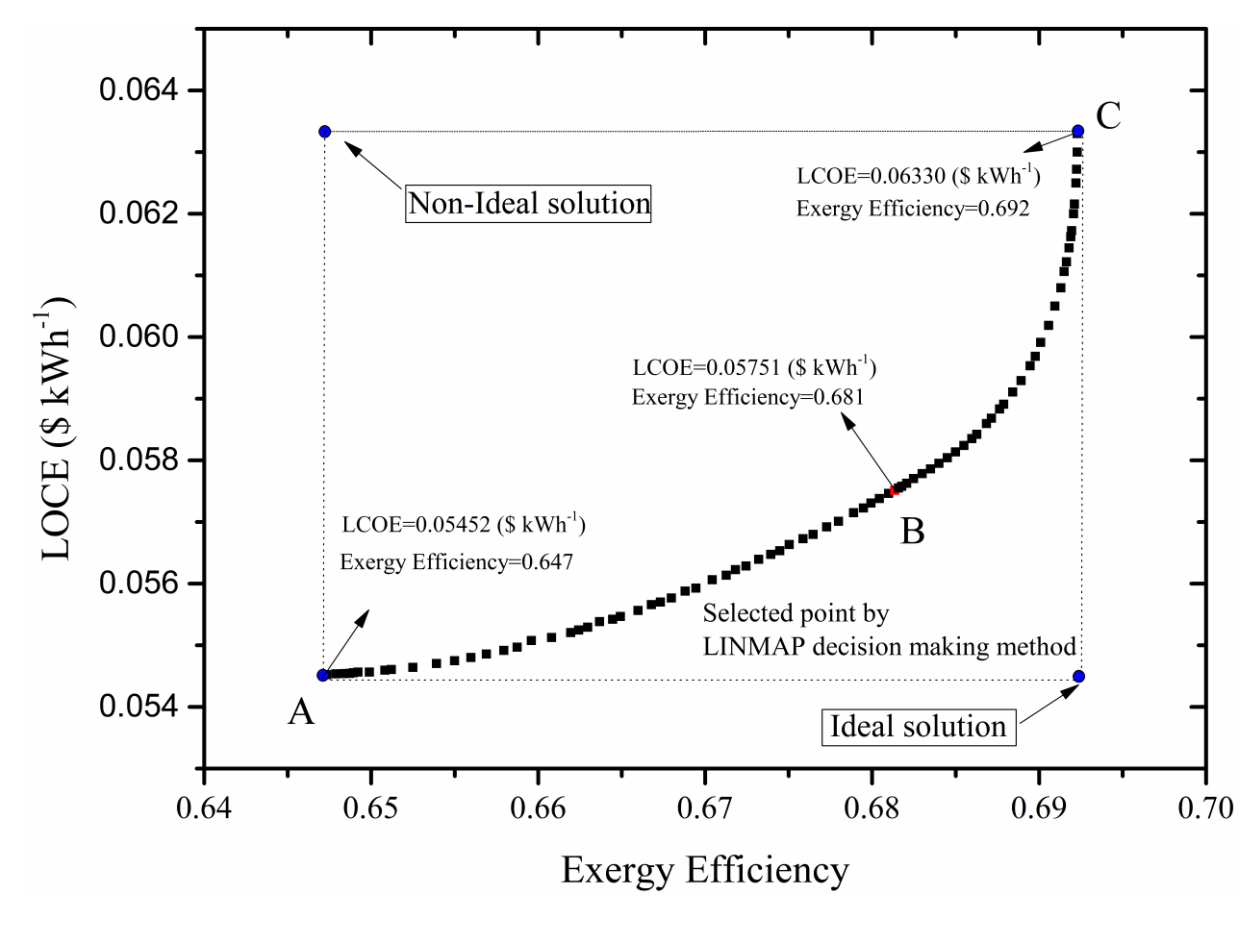


Fig. 11. Pareto frontier for integrated power system.

Table 6 Optimum values of objective functions and design variables for points A-C on the Pareto frontier of the bi-objective optimization.

	Unit	A	B (optimal)	C
Design variables				
P_{b}	MPa	25.00	25.00	23.44
SR_{SOFC}	_	0.5187	0.4815	0.4200
$\dot{N}_{{ m CO}_2}$	mol s ⁻¹	70.95	24.54	10.00
$SR_{\rm SCO2BC}$	_	0.9276	0.8598	0.7325
$\dot{N}_{ m f}$	mol s ⁻¹	7.892	4.690	4.5
$T_{ m SOFC}$	K	1076	1061	1187
$U_{ m f}$	_	0.7816	0.8633	0.8693
PR	_	5.766	4.626	5.414
Objective function				
LCOE	kWh^{-1}	0.05452	0.05751	0.06330
System exergy efficiency	%	64.73	68.14	69.23
Other performance				
SOFC exergy efficiency	%	43.83	53.89	54.37
SOFC-GT exergy	%	57.94	64.93	67.88

efficiency				
SOFC power generation	kW	2860	2090	2023
SOFC-GT net power	kW	3781	2518	2526
generation				
SCO ₂ BC net power	kW	443.3	124.1	50.03
generation				
System exergy	kW	1881	966.3	866.6
destruction				
System electrical	%	66.90	70.42	71.55
efficiency				

The second law analysis indicates the irreversibility of the main components in the combined system and evaluates their contributions to the total exergy destruction. The corresponding exergy destruction rate at point B is presented in Fig. 12. It is obvious that the exergy destruction rate of the combustion chamber accounts for the largest proportion (33.99%) due to the fact that the combustion reactions are the source of irreversibility. The SOFC stack has the next highest exergy destruction rate (29.96%). The result is conform with that in Ref [8]. It is noteworthy that preheater 2, which is used for preheating the water, takes up the largest exergy destruction proportion (12.64%) among heat exchangers in entire system. The main thermal irreversibility, including both internal and external irreversibility, comes from the phase transition process [62].

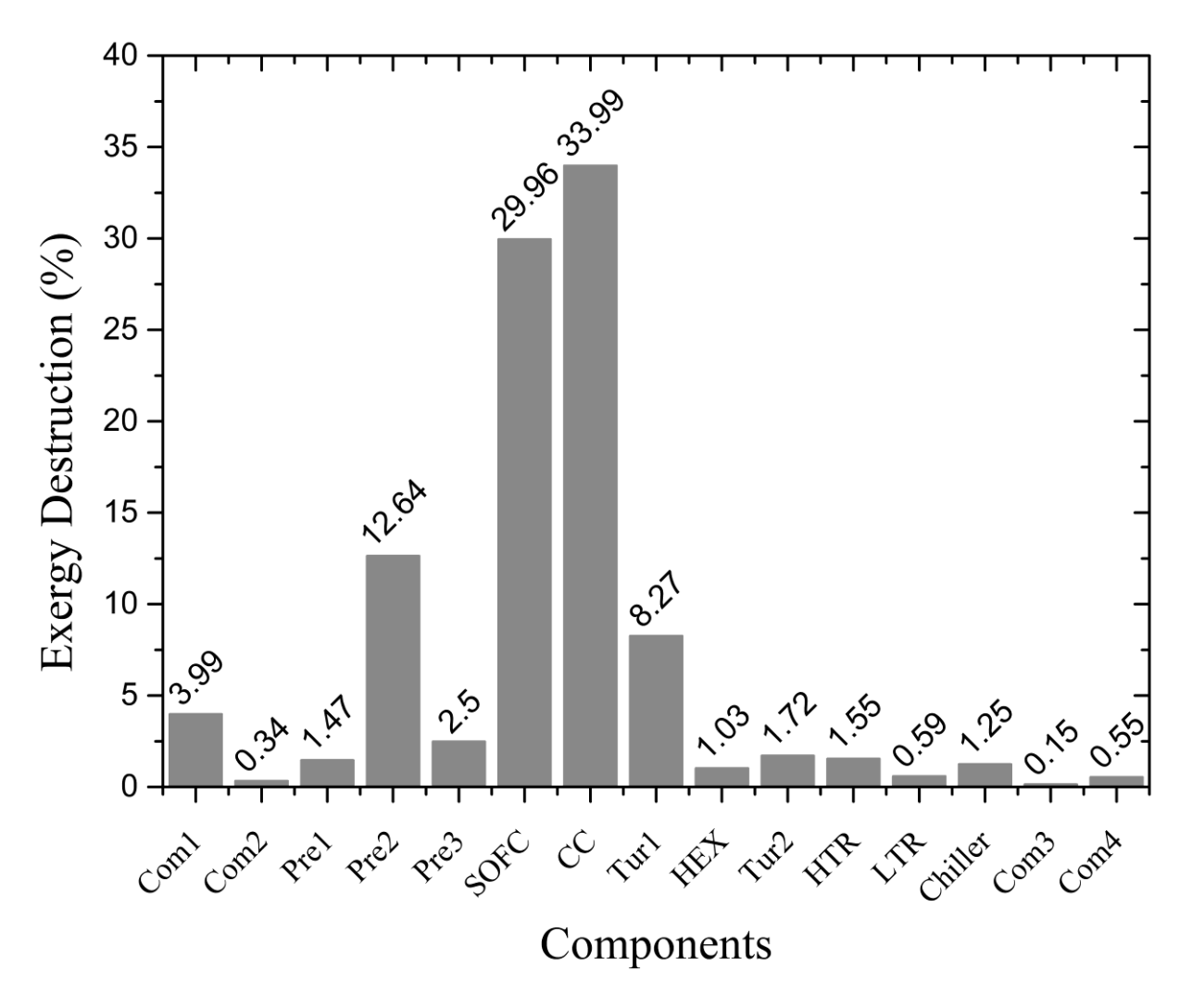


Fig. 12. The relative exergy destruction rate (%) of various components.

The distributions of eight design variables corresponding to the Pareto frontier of the combined system are shown in Fig. 13. The region of design variables is restricted by their upper and lower bounds (dashed line). It can be noted from Fig. 13(a) that the optimum values of turbine 2 entrance pressure are located near the upper bound, and most are on the upper limit of 25 MPa. The optimum splitter 2 ratio have a dispersive distribution in the range of 0.42-0.52. Moreover, as shown in Fig. 13(b), the optimum values of the fuel molar flowrate varies in the range of 4.5 mol s⁻¹ -7.9 mol s⁻¹. In addition, the optimum values of the SOFC operating temperature can be found between 1060 K and 1190 K, mainly concentrated around

1070 K. Fig. 13(c) indicates that the utilization of fuel in the SOFC stack is typically within the range of 0.78-0.87 and the turbine 1 pressure ratio are ever distributed in the range of 4.4-5.8, close to the lower bound. Furthermore, as shown in Fig. 13(d), the optimum CO₂ molar flowrate almost fall in the whole range (10 mol s⁻¹ - 71 mol s⁻¹), while the optimum values of splitter 1 ratio vary from 0.73 to 0.93. In general, higher values of turbine 1 pressure ratio will result in a deviation from the optimum performance. To operate at better conditions, more molar flowrate of exhaust should be assigned to the preheater 2 for air preheating. Combined with the sensitive analysis in section 4.2, the values of SOFC operating temperature have much more obvious impacts on system performance compared with other design variables.



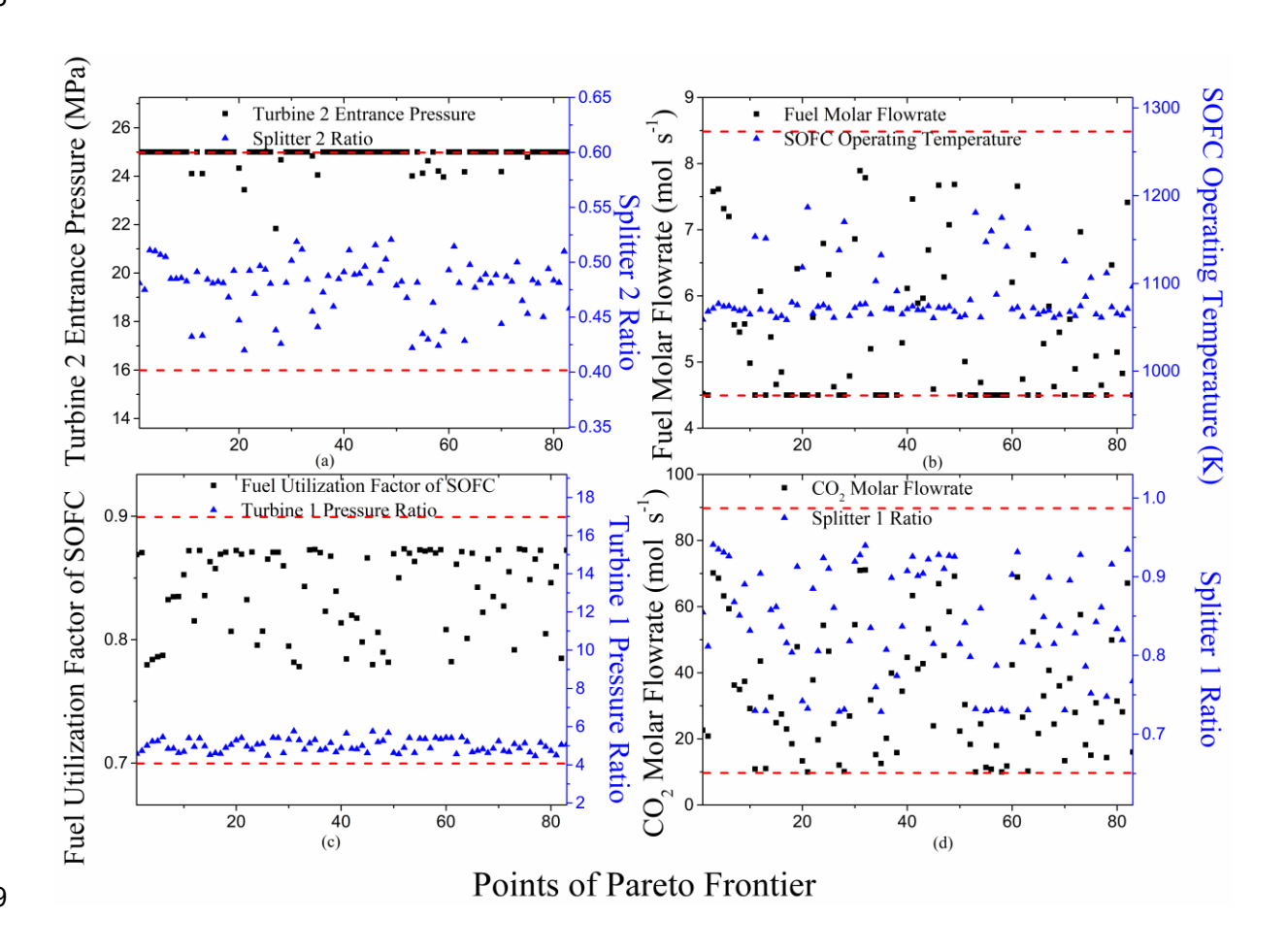


Fig. 13. Scattered distribution of (a) the turbine 2 entrance pressure and splitter 2 ratio, (b) the fuel molar flowrate and SOFC operating temperature, (c) the utilization factor of the SOFC and turbine 1 pressure ratio, (d) the CO₂ molar flowrate and splitter 1 ratio for the combined system with population in Pareto frontier.

5. Conclusions

A novel solid oxide fell cell-gas turbine-supercritical carbon dioxide Brayton cycle (SOFC-GT-SCO₂BC) combined system model is proposed with the objective to maximize the exergy efficiency and minimize the levelized cost of electricity (LCOE). Exergoeconomic analysis of several key parameters and the Pareto optimization are conducted, accordingly. Several conclusions can be drawn as follows:

- (1) The integration of SOFC-GT with a SCO₂BC can recover the waste heat from the GT exhaust and effectively improve the output power, exergy efficiency as well as reduce the LCOE. The maximum exergy efficiency increase by adding the bottoming cycle into the system exergy efficiency reaches 11.7%. The LINMAP decision-making method is utilized to select the optimum point from the Pareto frontier, which corresponds to a combined systemic exergy efficiency of 68.14% and the LCOE of 0.05751 (\$ kWh⁻¹). The exergy efficiency is considerable compared with conventional and some hybrid system have been published.
- (2) Single-parameter sensitivity analysis have been conducted for the exergy efficiency and LCOE against several key parameters individually. The two key parameters of the bottoming SCO₂BC have less impact on the entire system performance than upstream cycle's parameters. The combined system will reach a higher exergy efficiency with less consumption

of the fuel. Several extreme values for the output power, exergy efficiency, and LCOE exist in the sensitive curves with respect to the turbine1 pressure ratio, the operating temperature and the utilization factor of the SOFC stack. Meanwhile, due to the monotonic sensitive correlation, higher values of the turbine 2 inlet pressure and/or the split ratio of splitter 1 will increase the performance of the system.

(3) A significant tradeoff between the exergy efficiency and the LCOE is observed when optimizing the system design by multi-objective optimizations. With the increase of the exergy efficiency, the LCOE will increase moderately at first and increase sharply afterward. A fourth-order polynomial function is applied to fit the relationship between the LCOE and the exergy efficiency for the case of this SOFC-GT-SCO₂BC system's designer and engineer.

Overall, the proposed methodology provides a framework to optimize the design of SOFC-GT-SCO₂BC combined system with bi-objectives. Future work will compare the coupling effects of different bottoming cycles whose source temperature is low or medium such as Organic Rankine Cycle and Kalina Cycle, and explore the optimal system designs accordingly. In addition, the scaling effects of such combined system will be investigated to make the results more general and widely applicable.

Acknowledgement

The authors are grateful for the support from National Natural Science Foundation of China under grant No. 51876181. The work is also supported by the Science and Technology Planning Projects of Fujian Province, China with grant No. 2018H00

Appendix A.
 Energy relations for the main components of the SOFC-GT-SCO₂BC system.

Component	Energy equations	
Combustion chamber	$\dot{n}_{11}h_{11} + \dot{n}_{12}h_{12} - \dot{Q}_{loss} = \dot{n}_{13}h_{13}, \dot{Q}_{loss} = \dot{n}_{11} \times (1 - \eta_{CC}) \times LHV$	(A.1)
Turbine 1	$ \eta_{\text{is,tur1}} = \frac{h_{13} - h_{14}}{h_{13} - h_{14'}}, \dot{W}_{\text{tur1}} = \dot{n}_{13}(h_{13} - h_{14}) $	(A.2)
Turbine 2	$ \eta_{\text{is,tur}2} = \frac{h_{\text{b}} - h_{\text{c}}}{h_{\text{b}} - h_{\text{c}}}, \dot{W}_{\text{tur}2} = \dot{n}_{\text{a}}(h_{\text{b}} - h_{\text{c}}) $	(A.3)
Pump	$ \eta_{\text{is,pump}} = \frac{h'_4 - h_3}{h_4 - h_3} , \dot{W}_{\text{pump}} = \dot{n}_5 (h_6 - h_5) $	(A.4)
Compressor 1	$ \eta_{\text{is,com1}} = \frac{h'_2 - h_1}{h_2 - h_1} , \dot{W}_{\text{com1}} = \dot{n}_1 (h_2 - h_1) $	(A.5)
Compressor 2	$ \eta_{\text{is,com2}} = \frac{h'_6 - h_5}{h_6 - h_5} , \dot{W}_{\text{com2}} = \dot{n}_5 (h_6 - h_5) $	(A.6)
Compressor 3	$ \eta_{\text{is,com3}} = \frac{h'_{\text{h}} - h_{\text{g}}}{h_{\text{h}} - h_{\text{g}}} , \dot{W}_{\text{com3}} = \dot{n}_{\text{g}} (h_{\text{h}} - h_{\text{g}}) $	(A.7)
Compressor 4	$ \eta_{\text{is,com}4} = \frac{h'_{\text{k}} - h_{\text{j}}}{h_{\text{k}} - h_{\text{j}}} , \dot{W}_{\text{com}4} = \dot{n}_{\text{j}} (h_{\text{k}} - h_{\text{j}}) $	(A.8)
HEX	$\dot{n}_{13}(h_{14} - h_{15}) = \dot{n}_{a}(h_{b} - h_{a})$	(A.9)
HTR	$\dot{n}_{\rm c}(h_{\rm c}-h_{\rm d})=\dot{n}_{\rm a}(h_{\rm a}-h_{\rm l})$	(A.10)
LTR	$\dot{n}_a(h_{\rm d} - h_{\rm e}) = \dot{n}_{\rm g}(h_{\rm i} - h_{\rm h})$	(A.11)
Chiller	$\dot{n}_{\rm g}(h_{\rm f} - h_{\rm g}) = \dot{n}_{\rm m}(h_{\rm n} - h_{\rm m})$	(A.12)
Splitter 1	$\dot{n}_{\rm e}h_{\rm e}=\alpha\dot{n}_{\rm e}h_{\rm f}+(1-\alpha)\dot{n}_{\rm e}h_{\rm j}$	(A.13)

Appendix B.
 Exergy relations for the main components of the SOFC-GT- SCO₂BC system.

Components	Equation	
Compressor 1	$\dot{E}_{\rm x,dest,com1} = \dot{E}_1 - \dot{E}_2 + \dot{W}_{\rm com1}$	(B.1)
Compressor 2	$\dot{E}_{\rm x,dest,com2} = \dot{E}_5 - \dot{E}_6 + \dot{W}_{\rm com2}$	(B.2)
Pump	$\dot{E}_{ m x,dest,pump} = \dot{E}_3 - \dot{E}_4 + \dot{W}_{ m pump}$	(B.3)
Preheater 1	$\dot{E}_{\text{x,dest,pre1}} = \dot{E}_6 + \dot{E}_{15} - (\dot{E}_9 + \dot{E}_{16})$	(B.4)
Preheater 2	$\dot{E}_{\text{x,dest,pre2}} = \dot{E}_{17} + \dot{E}_4 - (\dot{E}_{20} + \dot{E}_8)$	(B.5)
Preheater 3	$\dot{E}_{\text{x,dest,pre}3} = \dot{E}_2 + \dot{E}_{18} - (\dot{E}_7 + \dot{E}_{19})$	(B.6)
SOFC	$\dot{E}_{\text{x,dest,SOFC}} = (\dot{E}_7 + \dot{E}_{10}) - (\dot{E}_{11} + \dot{E}_{12}) - \dot{W}_{\text{SOFC,DC}}$	(B.7)
Combustion chamber	$\dot{E}_{\text{x,dest,CC}} = (\dot{E}_{11} + \dot{E}_{12}) - \dot{E}_{13} - \dot{Q}_{\text{CC}} (1 - \frac{T_0}{T_{\text{CC}}})$	(B.8)
Turbine 1	$\dot{E}_{\mathrm{x,dest,tur1}} = \dot{E}_{\mathrm{13}} - \dot{E}_{\mathrm{14}} - \dot{W}_{\mathrm{tur1}}$	(B.9)
HEX	$\dot{E}_{\rm x,dest,HEX} = \dot{E}_{\rm 14} + \dot{E}_{\rm a} - (\dot{E}_{\rm 15} + \dot{E}_{\rm b})$	(B.10)
Turbine 2	$\dot{E}_{\rm x,dest,tur2} = \dot{E}_{\rm b} - \dot{E}_{\rm c} - \dot{W}_{\rm tur2}$	(B.11)
HTR	$\dot{E}_{\mathrm{x,dest,HTR}} = \dot{E}_{\mathrm{c}} + \dot{E}_{l} - (\dot{E}_{\mathrm{d}} + \dot{E}_{\mathrm{a}})$	(B.12)
LTR	$\dot{E}_{\mathrm{x,dest,LTR}} = \dot{E}_{\mathrm{d}} + \dot{E}_{\mathrm{h}} - (\dot{E}_{\mathrm{i}} + \dot{E}_{\mathrm{e}})$	(B.13)
Compressor 3	$\dot{E}_{\rm x,dest,com3} = \dot{E}_{\rm g} - \dot{E}_{\rm h} + \dot{W}_{\rm com3}$	(B.14)
Compressor 4	$\dot{E}_{\mathrm{x,dest,com4}} = \dot{E}_{\mathrm{j}} - \dot{E}_{\mathrm{k}} + \dot{W}_{\mathrm{com4}}$	(B.15)
Chiller	$\dot{E}_{\text{x,dest,chiller}} = \dot{E}_{\text{f}} + \dot{E}_{\text{m}} - (\dot{E}_{\text{g}} + \dot{E}_{\text{n}})$	(B.16)

Appendix C.
 The temperature, pressure, and molar flowrate of nodes in Fig. 1 for the optimum result.

Nodo	T/V	D/MD _o	Molar flowrate/mol s ⁻¹						
Node	T/K	P/MPa	CH ₄	H_2	CO	CO_2	H_2O	N_2	O_2
1	298.15	0.10	0.00	0.00	0.00	0.00	0.00	46.65	13.40
2	495.24	0.47	0.00	0.00	0.00	0.00	0.00	46.65	13.40
3	298.15	0.10	0.00	0.00	0.00	0.00	10.32	0.00	0.00
4	298.20	0.47	0.00	0.00	0.00	0.00	10.32	0.00	0.00
5	298.15	0.10	4.69	0.00	0.00	0.00	0.00	0.00	0.00
6	439.90	0.47	4.69	0.00	0.00	0.00	0.00	0.00	0.00
7	774.02	0.47	0.00	0.00	0.00	0.00	0.00	46.65	13.40
8	774.18	0.47	0.00	0.00	0.00	0.00	10.32	0.00	0.00
9	774.18	0.47	4.69	0.00	0.00	0.00	0.00	0.00	0.00
10	774.18	0.47	4.69	0.00	0.00	0.00	10.32	0.00	0.00
11	1061.38	0.47	0.00	2.48	0.58	4.11	17.17	0.00	0.00
12	1061.38	0.47	0.00	0.00	0.00	0.00	0.00	46.65	4.59
13	1326.99	0.47	0.00	0.00	0.00	4.68	19.66	46.65	3.06
14	1040.95	0.10	0.00	0.00	0.00	4.68	19.66	46.65	3.06
15	936.37	0.10	0.00	0.00	0.00	4.68	19.66	46.65	3.06
16	905.06	0.10	0.00	0.00	0.00	4.68	19.66	46.65	3.06
17	905.06	0.10	0.00	0.00	0.00	2.25	9.47	22.47	1.47
18	905.06	0.10	0.00	0.00	0.00	2.43	10.19	24.18	1.59
19	515.36	0.10	0.00	0.00	0.00	2.43	10.19	24.18	1.59
20	373.19	0.10	0.00	0.00	0.00	2.25	9.47	22.47	1.47
21	447.35	0.10	0.00	0.00	0.00	4.68	19.66	46.65	3.06
a	785.19	25.00	0.00	0.00	0.00	24.54	0.00	0.00	0.00
b	990.95	25.00	0.00	0.00	0.00	24.54	0.00	0.00	0.00
c	849.22	7.39	0.00	0.00	0.00	24.54	0.00	0.00	0.00
d	516.10	7.39	0.00	0.00	0.00	24.54	0.00	0.00	0.00
e	393.84	7.39	0.00	0.00	0.00	24.54	0.00	0.00	0.00
f	392.49	7.39	0.00	0.00	0.00	21.10	0.00	0.00	0.00
g	305.00	7.39	0.00	0.00	0.00	21.10	0.00	0.00	0.00
h	383.84	25.00	0.00	0.00	0.00	21.10	0.00	0.00	0.00
i	480.13	25.00	0.00	0.00	0.00	21.10	0.00	0.00	0.00
j	393.84	7.39	0.00	0.00	0.00	3.44	0.00	0.00	0.00
k	526.16	25.00	0.00	0.00	0.00	3.44	0.00	0.00	0.00
1	486.38	25.00	0.00	0.00	0.00	24.54	0.00	0.00	0.00

References

- [1] EG&G Servise. Parsons. Fuel cell handbook. 7th ed. West Virginia, USA: U.S. Department of Energy; 2004.
- [2] P.J. Bessette NF. Status of Siemens Westinghouse tubular solid oxide fuel cell technology and development program. In: Proceedings of the 2000 fuel cell seminar, Courtesy Associates, November 2000. (2000).
- [3] C. Bao, Y. Shi, E. Croiset, C. Li, N. Cai. A multi-level simulation platform of natural gas internal reforming
 solid oxide fuel cell–gas turbine hybrid generation system: Part I. Solid oxide fuel cell model library.
 Journal of Power Sources. 195 (2010) 4871-92.
- [4] S.F. Sghaier, T. Khir, A. Ben Brahim. Energetic and exergetic parametric study of a SOFC-GT hybrid power plant. International Journal of Hydrogen Energy. 43 (2018) 3542-54.
- 700 [5] R.S. El-Emam, I. Dincer, G.F. Naterer. Energy and exergy analyses of an integrated SOFC and coal gasification system. International Journal of Hydrogen Energy. 37 (2012) 1689-97.
- [6] Y. Zhao, J. Sadhukhan, A. Lanzini, N. Brandon, N. Shah. Optimal integration strategies for a syngas fuelled
 SOFC and gas turbine hybrid. Journal of Power Sources. 196 (2011) 9516-27.
- 704 [7] J. Pirkandi, M. Mahmoodi, M. Ommian. An optimal configuration for a solid oxide fuel cell-gas turbine
 705 (SOFC-GT) hybrid system based on thermo-economic modelling. Journal of Cleaner Production. 144 (2017)
 706 375-86.
- 707 [8] M. Shamoushaki, M.A. Ehyaei, F. Ghanatir. Exergy, economic and environmental analysis and multi-objective optimization of a SOFC-GT power plant. Energy. 134 (2017) 515-31.
- [9] L. Tan, X. Dong, Z. Gong, M. Wang. Investigation on performance of an integrated SOFC-GE-KC power
 generation system using gaseous fuel from biomass gasification. Renewable Energy. 107 (2017) 448-61.
- 711 [10] Z. Yan, P. Zhao, J. Wang, Y. Dai. Thermodynamic analysis of an SOFC–GT–ORC integrated power system with liquefied natural gas as heat sink. International Journal of Hydrogen Energy. 38 (2013) 3352-63.
- [11] S. Zhang, H. Liu, M. Liu, E. Sakaue, N. Li, Y. Zhao. An efficient integration strategy for a SOFC-GT-SORC combined system with performance simulation and parametric optimization. Applied Thermal Engineering.
 121 (2017) 314-24.
- [12] E. Gholamian, V. Zare. A comparative thermodynamic investigation with environmental analysis of SOFC
 waste heat to power conversion employing Kalina and Organic Rankine Cycles. Energy Conversion and
 Management. 117 (2016) 150-61.
- 719 [13] M.A. Ehyaei, M.A. Rosen. Optimization of a triple cycle based on a solid oxide fuel cell and gas and steam 720 cycles with a multiobjective genetic algorithm and energy, exergy and economic analyses. Energy 721 Conversion and Management. 180 (2019) 689-708.
- 722 [14] M. Ebrahimi, I. Moradpoor. Combined solid oxide fuel cell, micro-gas turbine and organic Rankine cycle for power generation (SOFC–MGT–ORC). Energy Conversion and Management. 116 (2016) 120-33.
- 724 [15] V. Eveloy, W. Karunkeyoon, P. Rodgers, A. Al Alili. Energy, exergy and economic analysis of an integrated solid oxide fuel cell gas turbine organic Rankine power generation system. International Journal of Hydrogen Energy. 41 (2016) 13843-58.
- 727 [16] A. Akkaya, B. Sahin, H. Huseyinerdem. An analysis of SOFC/GT CHP system based on exergetic performance criteria. International Journal of Hydrogen Energy. 33 (2008) 2566-77.
- [17] R. Ahmadi, S.M. Pourfatemi, S. Ghaffari. Exergoeconomic optimization of hybrid system of GT, SOFC and
 MED implementing genetic algorithm. Desalination. 411 (2017) 76-88.
- 731 [18] H.A. Reyhani, M. Meratizaman, A. Ebrahimi, O. Pourali, M. Amidpour. Thermodynamic and economic optimization of SOFC-GT and its cogeneration opportunities using generated syngas from heavy fuel oil gasification. Energy. 107 (2016) 141-64.

- 734 [19] Q. Meng, J. Han, L. Kong, H. Liu, T. Zhang, Z. Yu. Thermodynamic analysis of combined power generation
- system based on SOFC/GT and transcritical carbon dioxide cycle. International Journal of Hydrogen Energy.
 42 (2017) 4673-8.
- 737 [20] S. Ishiyama, Y. Muto, Y. Kato, S. Nishio, T. Hayashi, Y. Nomoto. Study of steam, helium and supercritical
- 738 CO₂ turbine power generations in prototype fusion power reactor. Progress in Nuclear Energy. 50 (2008)
 739 325-32.
- 740 [21] F. Crespi, G. Gavagnin, D. Sánchez, G.S. Martínez. Supercritical carbon dioxide cycles for power generation:
 741 A review. Applied Energy. 195 (2017) 152-83.
- 742 [22] F.A. Al-Sulaiman, M. Atif. Performance comparison of different supercritical carbon dioxide Brayton cycles integrated with a solar power tower. Energy. 82 (2015) 61-71.
- 744 [23] S. Hou, Y. Wu, Y. Zhou, L. Yu. Performance analysis of the combined supercritical CO₂ recompression and regenerative cycle used in waste heat recovery of marine gas turbine. Energy Conversion and Management. 151 (2017) 73-85.
- [24] D. Sánchez, J.M. Muñoz de Escalona, R. Chacartegui, A. Muñoz, T. Sánchez. A comparison between molten
 carbonate fuel cells based hybrid systems using air and supercritical carbon dioxide Brayton cycles with
 state of the art technology. Journal of Power Sources. 196 (2011) 4347-54.
- [25] M.A. Jokar, M.H. Ahmadi, M. Sharifpur, J.P. Meyer, F. Pourfayaz, T. Ming. Thermodynamic evaluation and multi-objective optimization of molten carbonate fuel cell-supercritical CO₂ Brayton cycle hybrid system.
 Energy Conversion and Management. 153 (2017) 538-56.
- 753 [26] Process Systems Enterprise Ltd., gPROMS Advanced User Guide. (2004).
- 754 [27] A.I. Kalina. Combined Cycle and Waste Heat Recovery Power Systems Based on a Novel Thermodynamic
 755 Energy Cycle Utilizing Low-Temperature Heat for Power Generation. Mechanical Engineering. 105 (1983)
 756 104-.
- 757 [28] P.P. Valdimarsson, L. Eliasson. Factors influencing the economics of the Kalina power cycle and situations758 of superior performance. 2003.
- 759 [29] S. Lecompte, H. Huisseune, M. van den Broek, B. Vanslambrouck, M. De Paepe. Review of organic 760 Rankine cycle (ORC) architectures for waste heat recovery. Renewable and Sustainable Energy Reviews. 47 761 (2015) 448-61.
- [30] G.R. Holcomb, C. Carney, Ö.N. Doğan. Oxidation of alloys for energy applications in supercritical CO₂ and
 H₂O. Corrosion Science. 109 (2016) 22-35.
- 764 [31] I.S. Muto Y, Kato Y, et al. Application of supercritical CO₂ gas turbine for the fossil fired thermal plant.
 765 Journal of Energy and Power Engineering. 4(9): 7-15 (2010).
- [32] D. Fiaschi, G. Manfrida, E. Rogai, L. Talluri. Exergoeconomic analysis and comparison between ORC and
 Kalina cycles to exploit low and medium-high temperature heat from two different geothermal sites. Energy
 Conversion and Management. 154 (2017) 503-16.
- [33] D. Ziviani, A. Beyene, M. Venturini. Advances and challenges in ORC systems modeling for low grade
 thermal energy recovery. Applied Energy. 121 (2014) 79-95.
- [34] B. Monje, D. Sánchez, M. Savill, P. Pilidis, T. Sánchez. A Design Strategy for Supercritical CO₂
 Compressors. Asme Turbo Expo: Turbine Technical Conference & Exposition2014.
- 773 [35] M. Valdés, R. Abbas, A. Rovira, J. Martín-Aragón. Thermal efficiency of direct, inverse and sCO₂ gas turbine cycles intended for small power plants. Energy. 100 (2016) 66-72.
- [36] Y. Ahn, S.J. Bae, M. Kim, S.K. Cho, S. Baik, J.I. Lee, et al. Review of supercritical CO₂ power cycle
 technology and current status of research and development. Nuclear Engineering and Technology. 47 (2015)
 647-61.

- 778 [37] C. Yue, D. Han, W. Pu, W. He. Comparative analysis of a bottoming transcritical ORC and a Kalina cycle for engine exhaust heat recovery. Energy Conversion and Management. 89 (2015) 764-74.
- 780 [38] E.P.B. Júnior, M.D.P. Arrieta, F.R.P. Arrieta, C.H.F. Silva. Assessment of a Kalina cycle for waste heat recovery in the cement industry. Applied Thermal Engineering. 147 (2019) 421-37.
- 782 [39] S. Quoilin, M. Orosz, H. Hemond, V. Lemort. Performance and design optimization of a low-cost solar organic Rankine cycle for remote power generation. Solar Energy. 85 (2011) 955-66.
- 784 [40] S. Glover, R. Douglas, M. De Rosa, X. Zhang, L. Glover. Simulation of a multiple heat source supercritical ORC (Organic Rankine Cycle) for vehicle waste heat recovery. Energy. 93 (2015) 1568-80.
- 786 [41] Y. Dai, J. Wang, L. Gao. Parametric optimization and comparative study of organic Rankine cycle (ORC) for low grade waste heat recovery. Energy Conversion and Management. 50 (2009) 576-82.
- 788 [42] Y. Le Moullec. Conceptual study of a high efficiency coal-fired power plant with CO₂ capture using a supercritical CO₂ Brayton cycle. Energy. 49 (2013) 32-46.
- 790 [43] D.F. Cheddie. Integration of A Solid Oxide Fuel Cell into A 10 MW Gas Turbine Power Plant. Energies. 3 (2010) 754-69.
- [44] A.V. Akkaya. Electrochemical model for performance analysis of a tubular SOFC. International Journal of
 Energy Research. 31 (2007) 79-98.
- [45] Y. Feng, Y. Zhang, B. Li, J. Yang, Y. Shi. Comparison between regenerative organic Rankine cycle (RORC)
 and basic organic Rankine cycle (BORC) based on thermoeconomic multi-objective optimization
 considering exergy efficiency and levelized energy cost (LEC). Energy Conversion and Management. 96
 (2015) 58-71.
- 798 [46] S. Wright, C. Davidson, W. Scammell. Thermo-economic analysis of four sCO₂ waste heat recovery power systems. Fifth International SCO₂ Symposium, San Antonio, TX, Mar2016. pp. 28-31.
- [47] J. Dyreby, S. Klein, G. Nellis, D. Reindl. Design Considerations for Supercritical Carbon Dioxide Brayton
 Cycles With Recompression. Journal of Engineering for Gas Turbines & Power. 136 (2014) 101701.
- 802 [48] W. Kim, Y.-J. Baik, S. Jeon, D. Jeon, C. Byon. A mathematical correlation for predicting the thermal performance of cross, parallel, and counterflow PCHEs. International Journal of Heat and Mass Transfer. 106 (2017) 1294-302.
- 805 [49] S. Sanaye, A. Katebi. 4E analysis and multi objective optimization of a micro gas turbine and solid oxide fuel cell hybrid combined heat and power system. Journal of Power Sources. 247 (2014) 294-306.
- [50] A. Shirazi, M. Aminyavari, B. Najafi, F. Rinaldi, M. Razaghi. Thermal–economic–environmental analysis
 and multi-objective optimization of an internal-reforming solid oxide fuel cell–gas turbine hybrid system.
 International Journal of Hydrogen Energy. 37 (2012) 19111-24.
- [51] J. Song, X. Li, X. Ren, C. Gu. Performance analysis and parametric optimization of supercritical carbon dioxide (S-CO₂) cycle with bottoming Organic Rankine Cycle (ORC). Energy. 143 (2018) 406-16.
- [52] W. Cheng, W. Huang, Y. Nian. Global parameter optimization and criterion formula of supercritical carbon dioxide Brayton cycle with recompression. Energy Conversion and Management. 150 (2017) 669-77.
- [53] A. Javanshir, N. Sarunac, Z. Razzaghpanah. Thermodynamic analysis of simple and regenerative Brayton
 cycles for the concentrated solar power applications. Energy Conversion and Management. 163 (2018)
 428-43.
- [54] J. Jia, Q. Li, M. Luo, L. Wei, A. Abudula. Effects of gas recycle on performance of solid oxide fuel cell power systems. Energy. 36 (2011) 1068-75.
- 819 [55] F.L. A. F. Massardo. Internal Reforming Solid Oxide Fuel Cell-Gas Turbine Combined Cycles 820 (IRSOFC-GT): Part A—Cell Model and Cycle Thermodynamic Analysis. Best Paper Award Cycle 821 Innovations Technical Committee.

- [56] Z. Liu, F. Forouzanfar, Y. Zhao. Comparison of SQP and AL algorithms for deterministic constrained
 production optimization of hydrocarbon reservoirs. Journal of Petroleum Science and Engineering. 171
 (2018) 542-57.
- [57] R. Jing, M. Wang, W. Wang, N. Brandon, N. Li, J. Chen, et al. Economic and environmental multi-optimal
 design and dispatch of solid oxide fuel cell based CCHP system. Energy Conversion and Management. 154
 (2017) 365-79.
- 828 [58] M.H. Ahmadi, A.H. Mohammadi, S. Dehghani, M.A. Barranco-Jiménez. Multi-objective 829 thermodynamic-based optimization of output power of Solar Dish-Stirling engine by implementing an 830 evolutionary algorithm. Energy Conversion and Management. 75 (2013) 438-45.
- 831 [59] M.H. Ahmadi, H. Hosseinzade, H. Sayyaadi, A.H. Mohammadi, F. Kimiaghalam. Application of the multi-objective optimization method for designing a powered Stirling heat engine: Design with maximized power, thermal efficiency and minimized pressure loss. Renewable Energy. 60 (2013) 313-22.
- 834 [60] Y. Li, S. Liao, G. Liu. Thermo-economic multi-objective optimization for a solar-dish Brayton system using NSGA-II and decision making. International Journal of Electrical Power & Energy Systems. 64 (2015) 167-75.
- 837 [61] M.A. Sienicki J, Dae Cho M.T., Vilim R., Momozaki Y., Lomperski S., Farmer M. Recent Research and B38 Development on the Supercritical Carbon Dioxide Brayton Cycle at Argonne National Laboratory.

 839 Supercritical CO2 Power Cycle Symposium 2009. (2009).
- [62] W. Gu, Y. Weng, Y. Wang, B. Zheng. Theoretical and experimental investigation of an organic Rankine cycle
 for a waste heat recovery system. Proceedings of the Institution of Mechanical Engineers, Part A: Journal of
 Power and Energy. 223 (2009) 523-33.

856 Figure captions:

- Fig. 1. The layout of a SOFC-GT- SCO₂BC combined system.
- Fig. 2. The T-S diagram of the bottoming SCO₂BC.
- Fig. 3. Flow chart of multi-objective NLP model solving procedure.
- Fig.4. Illustration of non-dominated and LINMAP decision-making approach.
- Fig.5. Effects of the fuel flowrate on the output power and the exergy destruction (a), the
- exergy efficiency and LCOE (b) for the combined system.
- Fig. 6. Effects of the pressure ratio of turbine 1 on different parameters for the combined
- system.
- Fig. 7. Effects of the SOFC stack operating temperature on different parameters for the
- 866 combined system.
- Fig. 8. Effects of the fuel utilization factor (U_f) on different parameters for the combined
- 868 system.
- Fig. 9. Effects of turbine 2 entrance pressure on different parameters for the combined system.
- Fig. 10. Effects of the split ratio of the SCO₂BC on different parameters for the combined
- 871 system.
- Fig. 11. Pareto frontier for integrated power system.
- Fig. 12. The relative exergy destruction rate (%) of various components.
- Fig. 13. Scattered distribution of (a) the turbine 2 entrance pressure and splitter 2 ratio, (b) the
- fuel molar flowrate and SOFC operating temperature, (c) the utilization factor of the SOFC
- and turbine 1 pressure ratio, (d) the CO₂ molar flowrate and splitter 1 ratio for the combined
- system with population in Pareto frontier.

878	Table captions:
879	Table 1 The characteristics of three common bottoming cycles.
880	Table 2 The cost functions of the equipment in SOFC-GT sub-system and SCO ₂ BC.
881	Table 3 Optimization constraints and ranges of design variables.
882	Table 4 Parameters setting in this simulation.
883	Table 5 Comparison of the simulation results of the SOFC-GT sub-system and the SCO ₂ BC
884	with the data obtained from references.
885	Table 6 Optimum values of objective functions and design variables for points A-C on the
886	Pareto frontier of the bi-objective optimization.

Table(s)

Table 1 The characteristics of three common bottoming cycles.

	Kalina Cycle	Organic Rankine Cyle	Supercritical CO ₂ Brayton Cycle
Heat source temperature	Low-medium temperature.	Low-medium temperature.	Medium-high temperature.
Working fluids	Ammonia-water mixture.	Organic fluid.	Carbon dioxide.
Advantages	Better coupling of temperatures between the working fluids and the source. Lower irreversibility in heat transfer process [27, 28].	Relatively compact system layout. Suitable working pressure, Especially suitable for the recovery and utilization of low-grade waste heat [29].	Good stability, Low corrosiveness, and environmental friendliness of working fluids [30]. Compact system layout [23]. High system efficiency [31].
Disadvantages	Additional shunt devices needed. High complexity of system, Poisonous and flammable working fluids [32].	Limited space for technics optimization. Environmental unfriendliness and toxicity of working fluids [33].	High requirements for equipment, especially compressors and turbines [34, 35]. Of most still in laboratory or demonstrations [21, 36].
Applications in coupling system	SOFC-GT [9, 12], Geothermal energy [32], Industrial waste heat [37, 38].	Solar energy [39], Geothermal energy [32], SOFC-GT [11, 14], Industrial waste heat [40, 41].	MCFC-GT [24, 25], Nuclear reactor[20], Industrial waste heat [42].

Table 2 The cost functions of the equipment in SOFC-GT sub-system and SCO₂BC.

Equipment	Cost function
SOFC-GT sub-system	
Gas turbine [50]	$\dot{W}_{\rm GT}(1318.5 - 98.328 \ln \dot{W}_{\rm GT})$
Compressor [50]	$91562(\frac{\dot{W}_{\rm com}}{445})^{0.67}$
Pump [50]	$705.48\dot{W}_{\text{pump}}^{0.71}(1+\frac{0.2}{1-\eta_{\text{pump}}})$
Fuel cell [17]	$S_{\text{SOFC}}(2.96T_{\text{SOFC}} - 1907)$
Electrical reformer [13, 17]	$10^5 (\frac{\dot{W}_{\rm SOFC,DC}}{500})^{0.7}$
Fuel cell auxiliaries [17]	$0.1C_{ m SOFC}$
Combustion chamber [18]	$(\frac{46.08\dot{m}_{\rm CC}}{0.995 - \frac{P_{\rm GT}}{P_{\rm CC}}})(1 + \exp(0.018T_{\rm GT} - 26.4))$
Preheater [18]	$8500 + 409(A_{\text{REC}}^{0.85})$
SCO ₂ BC	
Recuperator [46]	$2500(U \times A)_{REC}$
Heater [46]	$5000(U \times A)_{\text{HEX}}$
CO ₂ -chiller [46]	$1700(U \times A)_{\text{Chiller}}$
Turbomachinery+ Generator [46]	$600 \dot{W_{ m tur}}$

Table 3 Optimization constraints and ranges of design variables.

	– Unit	Description	Range of design variable	
	– Omi	Description	From	То
Constraint				
T _{pp} [16, 51, 52]	K	Pinch point temperature difference	10.00/20.00	-
$T_{ m min}$	K	The minimum temperature of exhaust gas	373	-
$T_{\rm TIT1}$ [50]	K	The inlet temperature of turbine 1		1550
T _{TIT2} [53]	K	The inlet temperature of turbine 2		1273
Design variables				
P _b [21, 23, 52]	MPa	Values of turbine 2 inlet pressure	16.0	25.0
SR_{SOFC}	-	The split ratio of splitter 2	0.300	0.700
$\dot{N}_{ m CO_2}$	mol s ⁻¹	Values of CO ₂ molar flowrate	10.0	80.0
SR _{SCO2BC} [23, 52]	-	The split ratio of splitter 1	0.650	0.980
$\dot{N}_{ m f}$ [10]	mol s ⁻¹	Values of fuel molar flowrate	4.50	8.50
T _{SOFC} [6, 44, 54]	K	The operating temperature of SOFC	973	1273
$U_{\rm f}[8, 12]$	-	The utilization factor of SOFC	0.700	0.900
PR [11, 55]	-	The pressure ratio of turbine 1	4.00	17.0

Table 4 Parameters setting in this simulation.

Term	Unit	Value
Ambient temperature [11]	K	298
Ambient pressure [23]	MPa	0.101
Fuel compressor isentropic efficiency [10]	%	82.0
Air compressor isentropic efficiency [10]	%	82.0
Pump efficiency [19]	%	80.0
Gas turbine isentropic efficiency [19]	%	75.0
Steam-to-carbon ratio [19]	-	2.20
Area of a cell [19]	cm ²	220
Cells number [19]	-	50,000
DC-AC inverter efficiency [14, 54]	%	95.0
Combustion chamber efficiency [19]	%	95.0
CO ₂ -turbine isentropic efficiency [52]	%	80.0
CO ₂ -compressor isentropic efficiency [52]	%	85.0
Pinch point temperature difference [10]	K	20.00
The recuperator effectiveness [14, 24]	%	92.0
CO ₂ -turbine outlet pressure [23]	MPa	7.40
Condenser inlet/outlet temperature [23]	K	298/320
$A_{\rm R}; A_{\rm S} [9, 17]$	-	-2.63×10 ⁻¹¹ ; 5.47×10 ⁻¹²
$B_{\rm R}; B_{\rm S} [9, 17]$	-	1.24×10 ⁻⁷ ; -2.57×10 ⁻⁸
$C_{\rm R}$; $C_{\rm S}$ [9, 17]	-	-2.25×10 ⁻⁴ ; 4.63×10 ⁻⁵
$D_{\rm R}; D_{\rm S}$ [9, 17]	-	1.95×10 ⁻¹ ; -3.91×10 ⁻²
$E_{\rm R}; E_{\rm S} [9, 17]$	-	-6.61×10; 1.32×10

Table(s)

Table 5 Comparison of the simulation results of the SOFC-GT sub-system and the SCO_2BC with the data obtained from references.

Parameter	Yan	Sienicki	Present	Difference
Farameter	[10]	[62]	work	(%)
Cell operating voltage (V)	0.614	-	0.626	2.11
SOFC (DC) power output (kW)	3126	-	3124	0.06
GT power output (kW)	1642	-	1698	3.41
SOFC electrical efficiency (%)	48.80	-	48.82	0.04
GT outlet temperature (K)	-	635.3	637.8	0.39
First law efficiency (%)	-	39.10	38.70	1.02

Table 6 Optimum values of objective functions and design variables for points A-C on the Pareto frontier of the bi-objective optimization.

	Unit	A	B (optimal)	С
Design variables				
P_{b}	MPa	25.00	25.00	23.44
SR_{SOFC}	-	0.5187	0.4815	0.4200
$\dot{N}_{{ m CO}_2}$	$mol s^{-1}$	70.95	24.54	10.00
$SR_{\rm SCO2BC}$	_	0.9276	0.8598	0.7325
$\dot{N}_{ m f}$	$mol s^{-1}$	7.892	4.690	4.5
$T_{ m SOFC}$	K	1076	1061	1187
$U_{ m f}$	_	0.7816	0.8633	0.8693
PR	-	5.766	4.626	5.414
Objective function				
LCOE	kWh^{-1}	0.05452	0.05751	0.06330
System exergy	%	64.73	68.14	69.23
efficiency				
Other performance				
SOFC exergy	%	43.83	53.89	54.37
efficiency				
SOFC-GT exergy	%	57.94	64.93	67.88
efficiency				
SOFC power	kW	2860	2090	2023
generation				
SOFC-GT net power	kW	3781	2518	2526
generation				
SCO ₂ BC net power	kW	443.3	124.1	50.03
generation				
System exergy	kW	1881	966.3	866.6
destruction				
System electrical	%	66.90	70.42	71.55
efficiency				

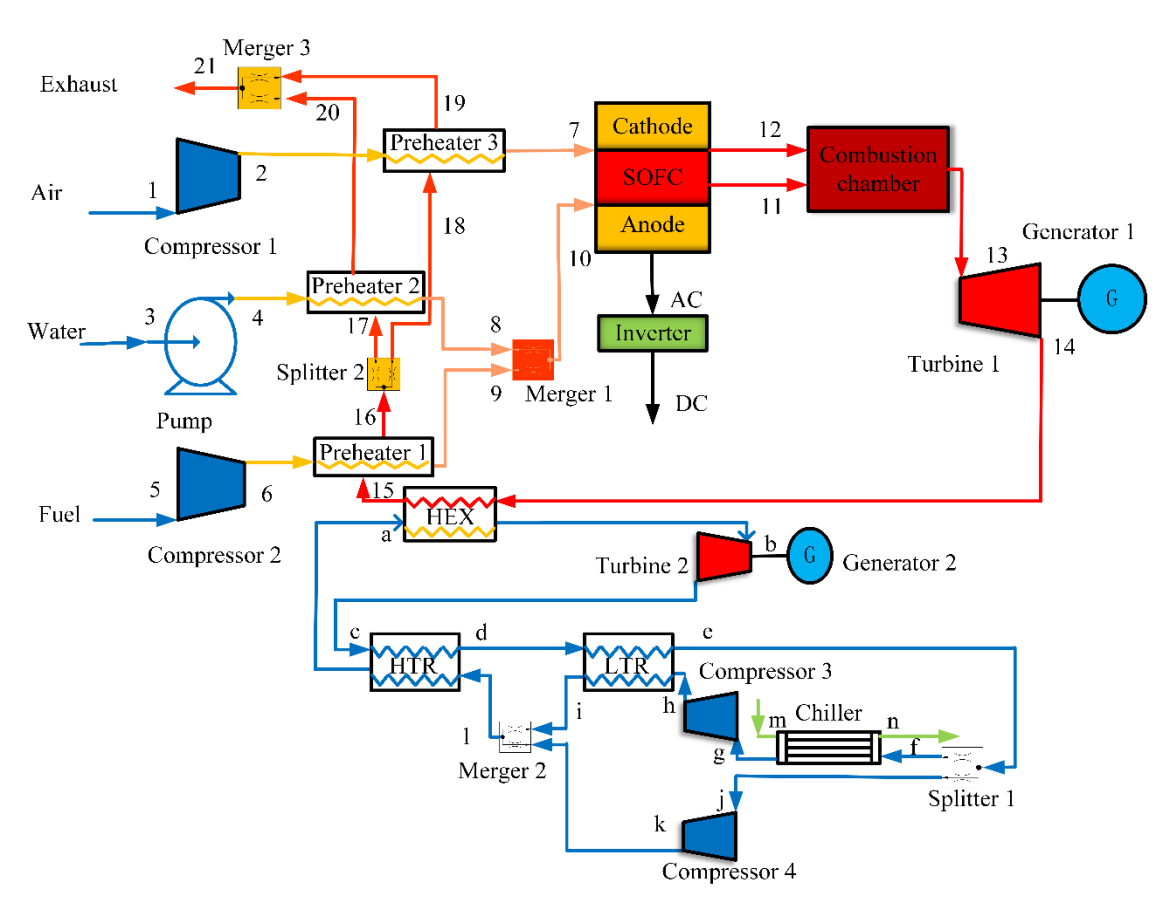


Fig. 1. The layout of a SOFC-GT- SCO₂BC combined power system.

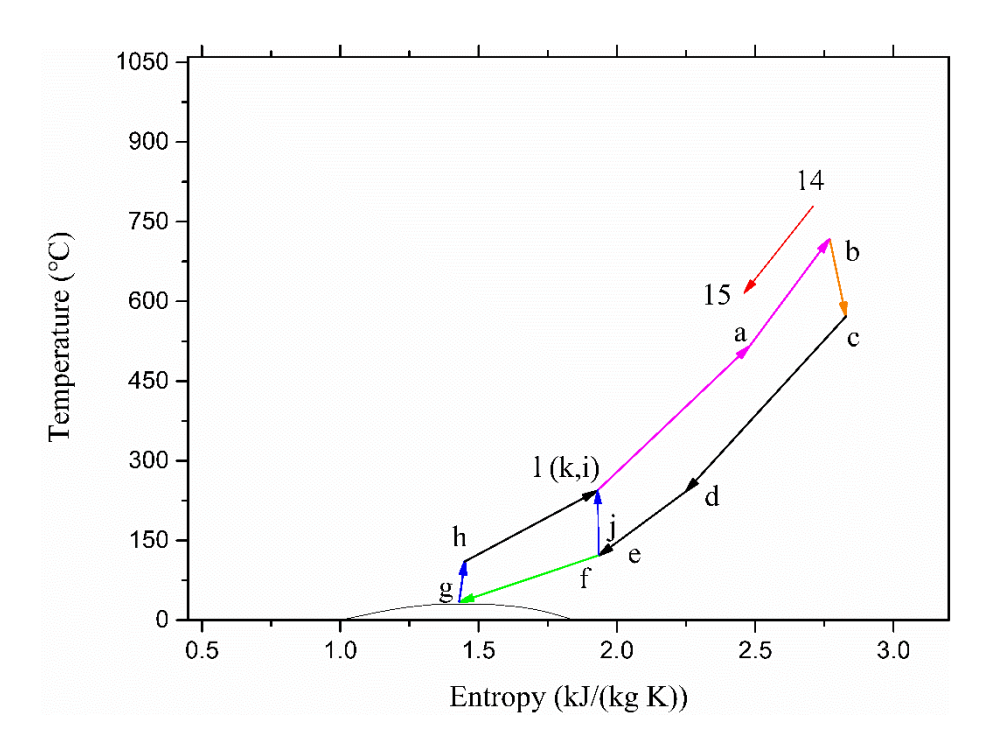


Fig. 2. The T-S diagram of the bottoming SCO₂BC.

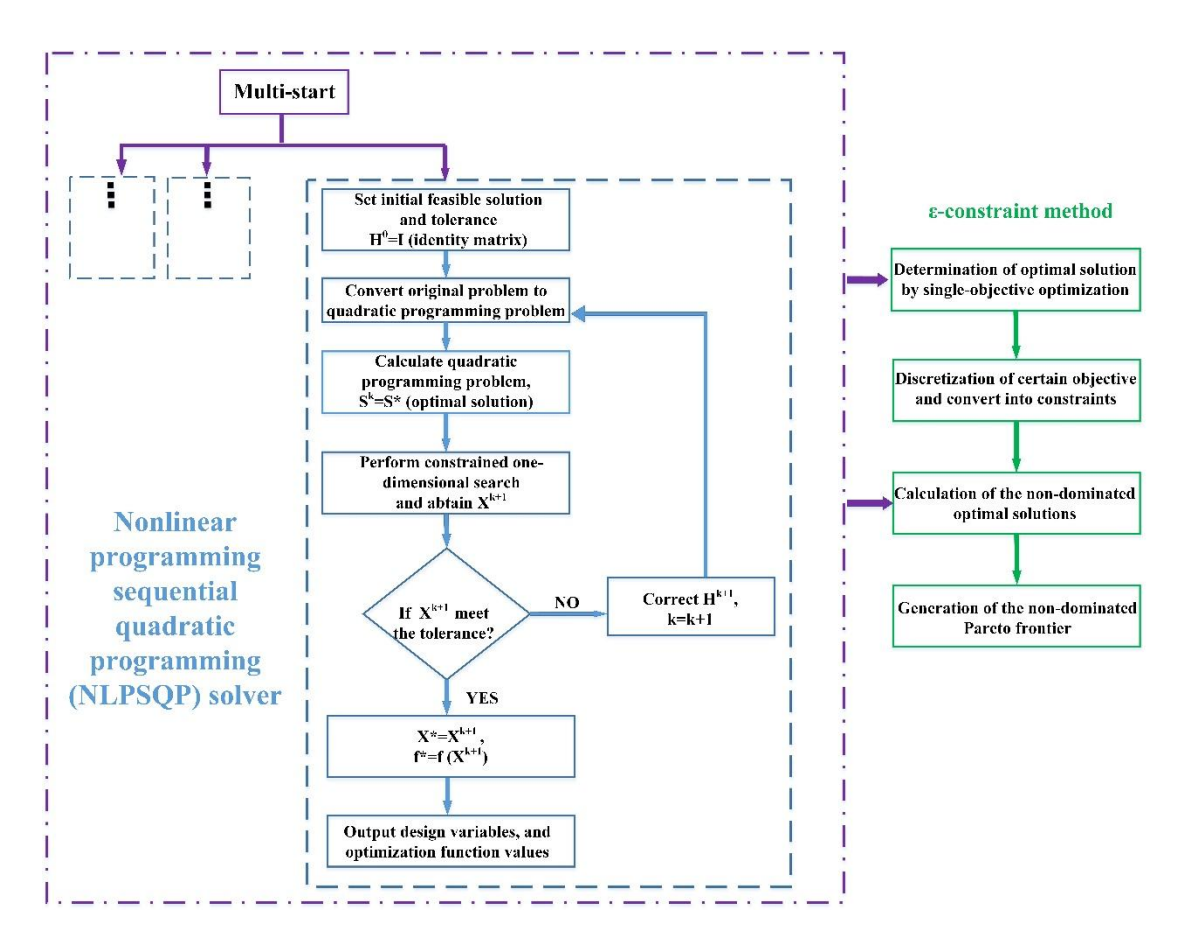


Fig. 3. Flow chart of multi-objective NLP model solving procedure.

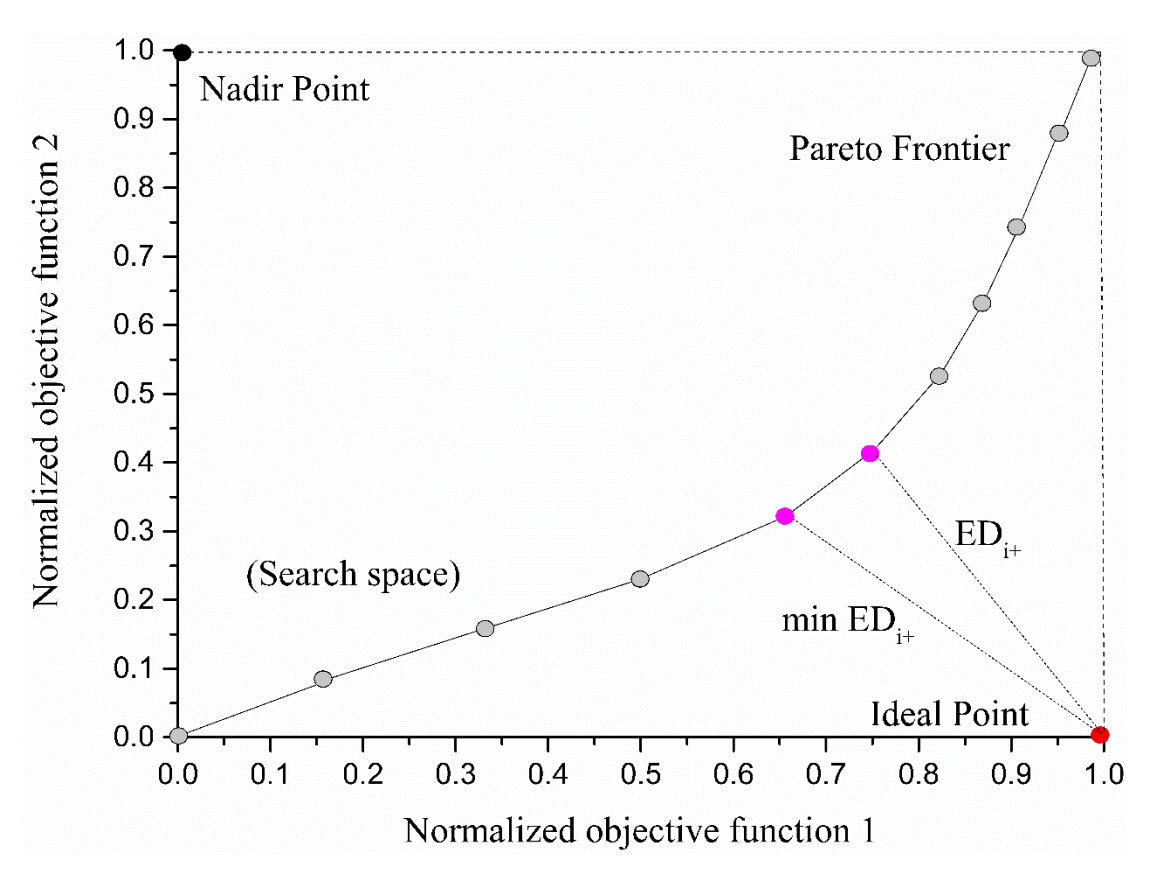


Fig. 4. Illustration of non-dominated and LINMAP decision-making approach.

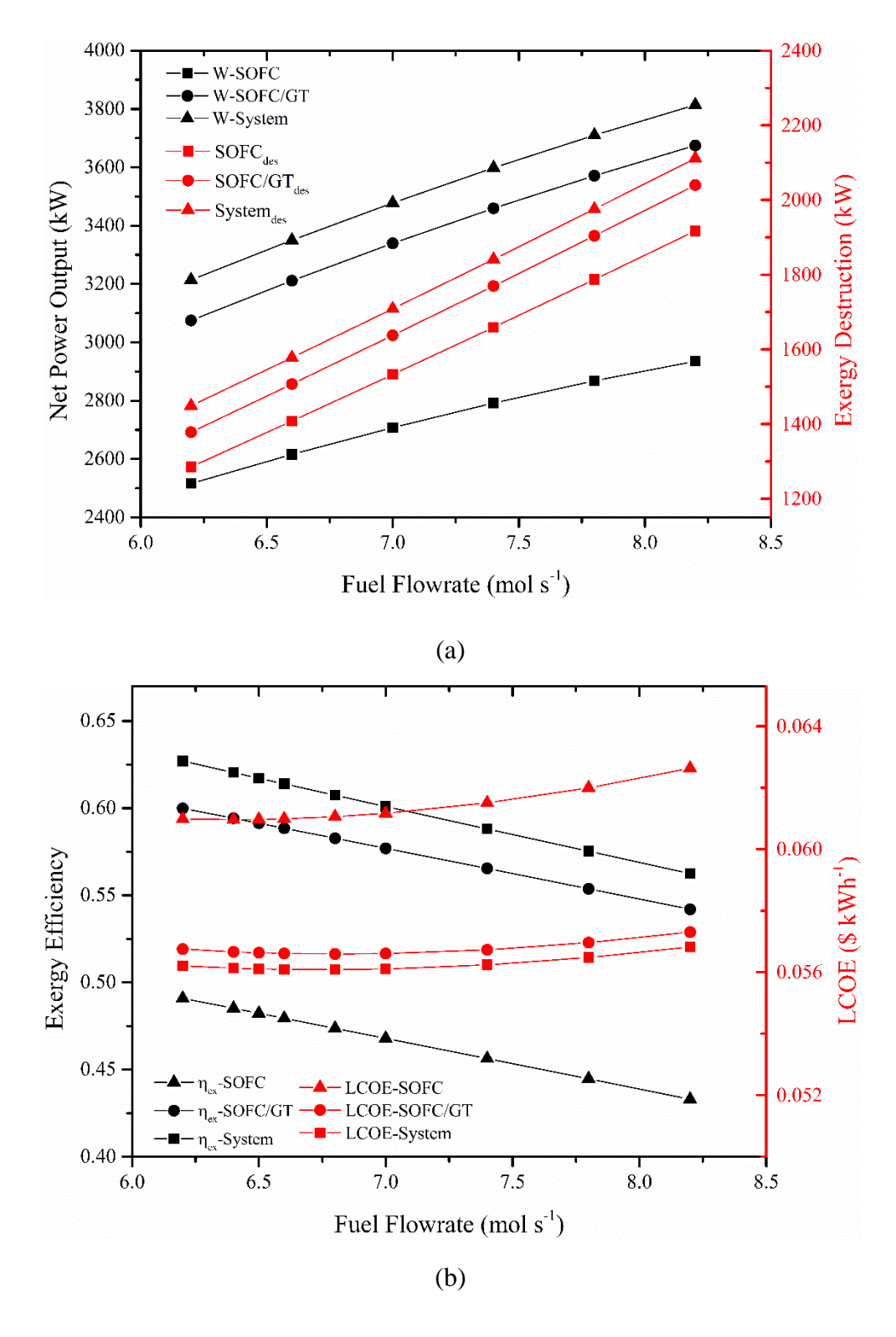


Fig. 5. Effects of the fuel flowrate on the output power and exergy destruction (a), the exergy efficiency and LCOE (b) for the combined system.

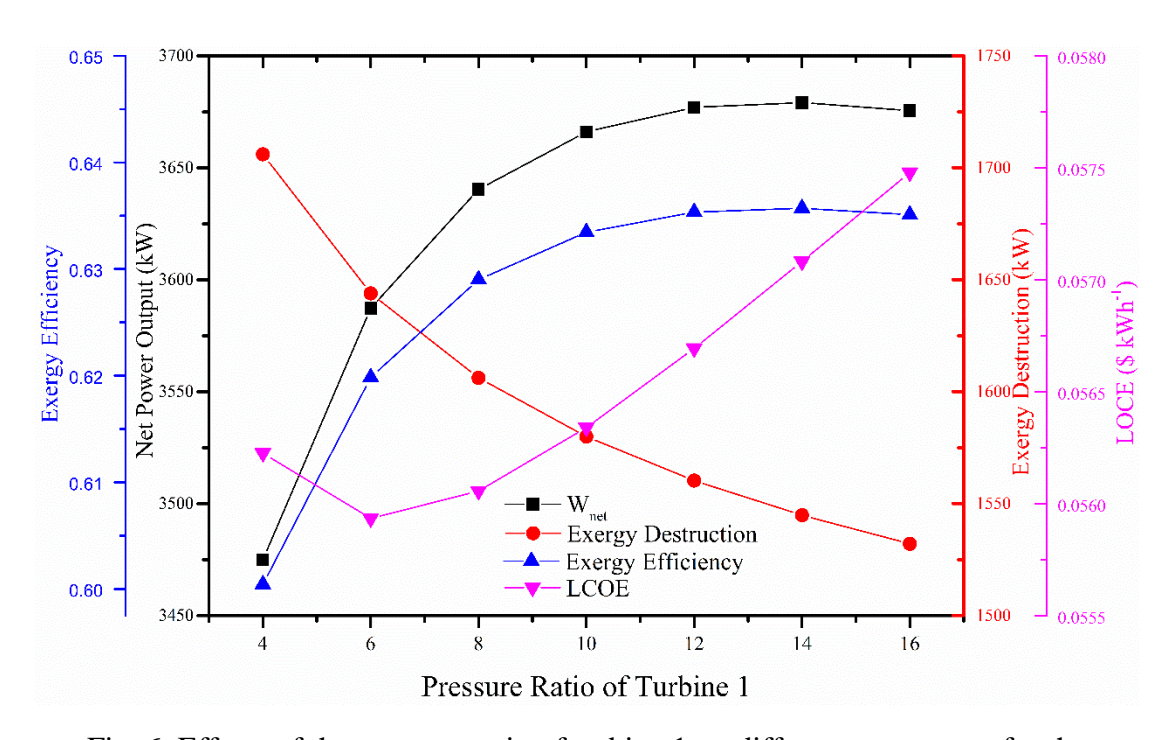


Fig. 6. Effects of the pressure ratio of turbine 1 on different parameters for the combined system.

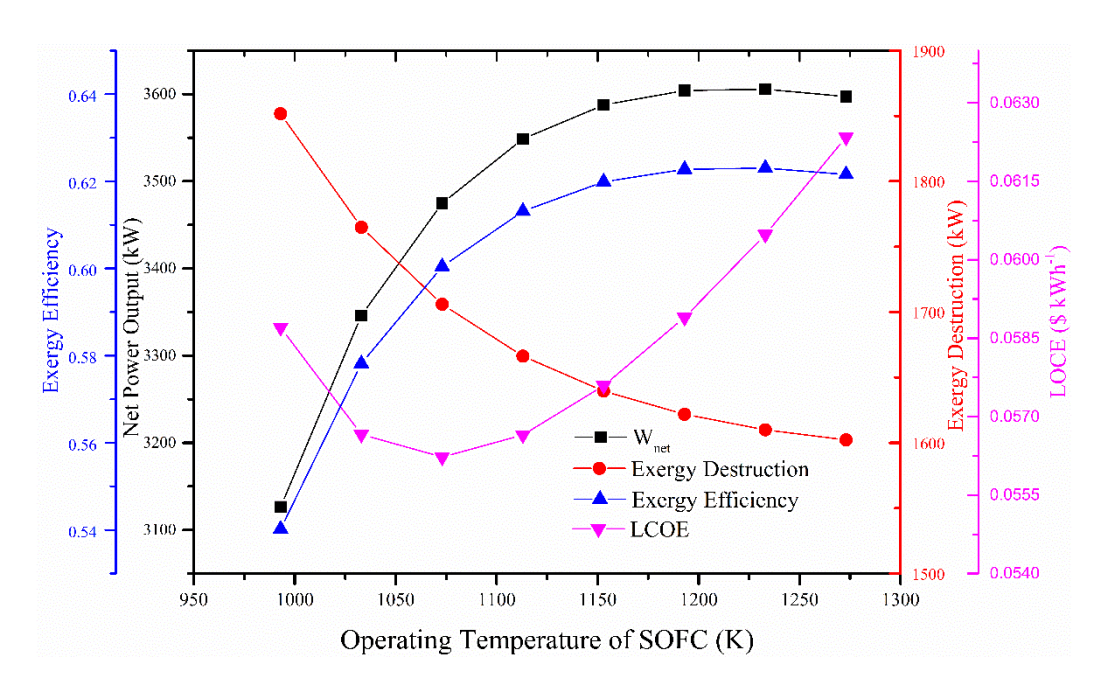


Fig. 7. Effects of the SOFC stack operating temperature on different parameters for the combined system.

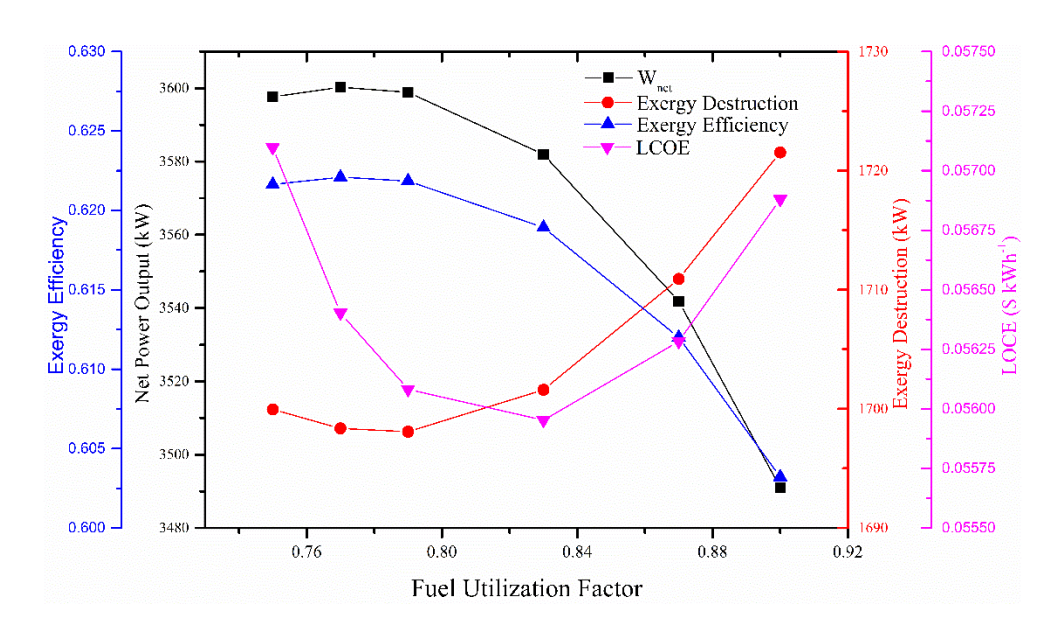


Fig. 8. Effects of the fuel utilization factor ($U_{\rm f}$) on different parameters for the combined system.

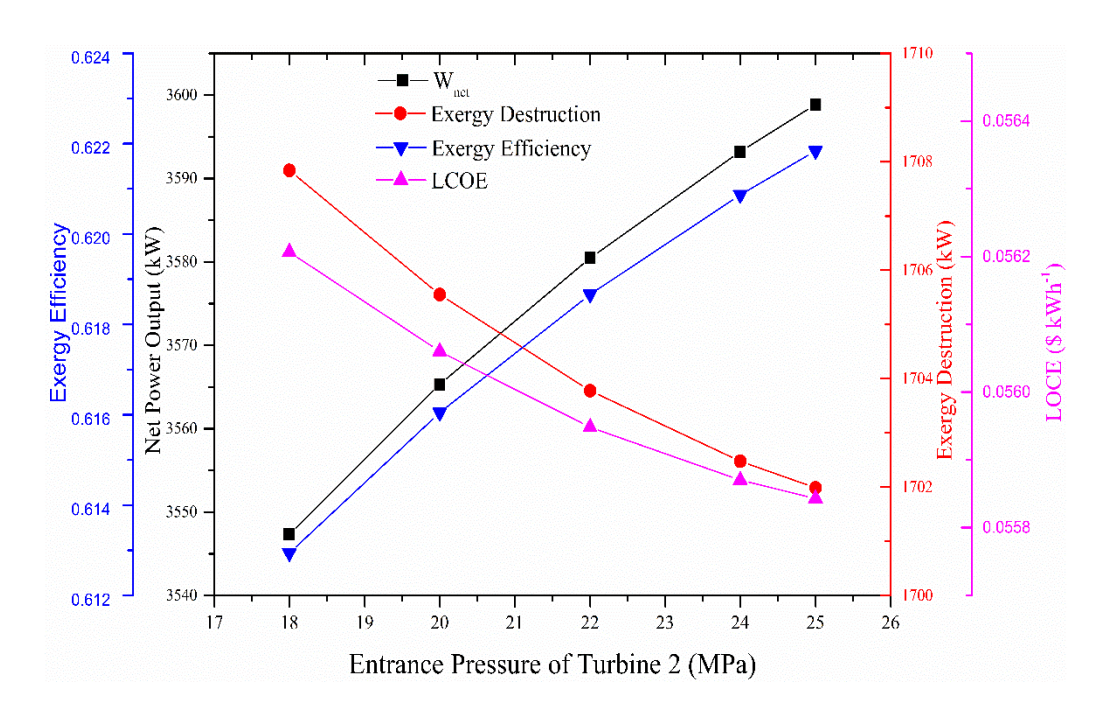


Fig. 9. Effects of turbine 2 entrance pressure on different parameters for the combined system.

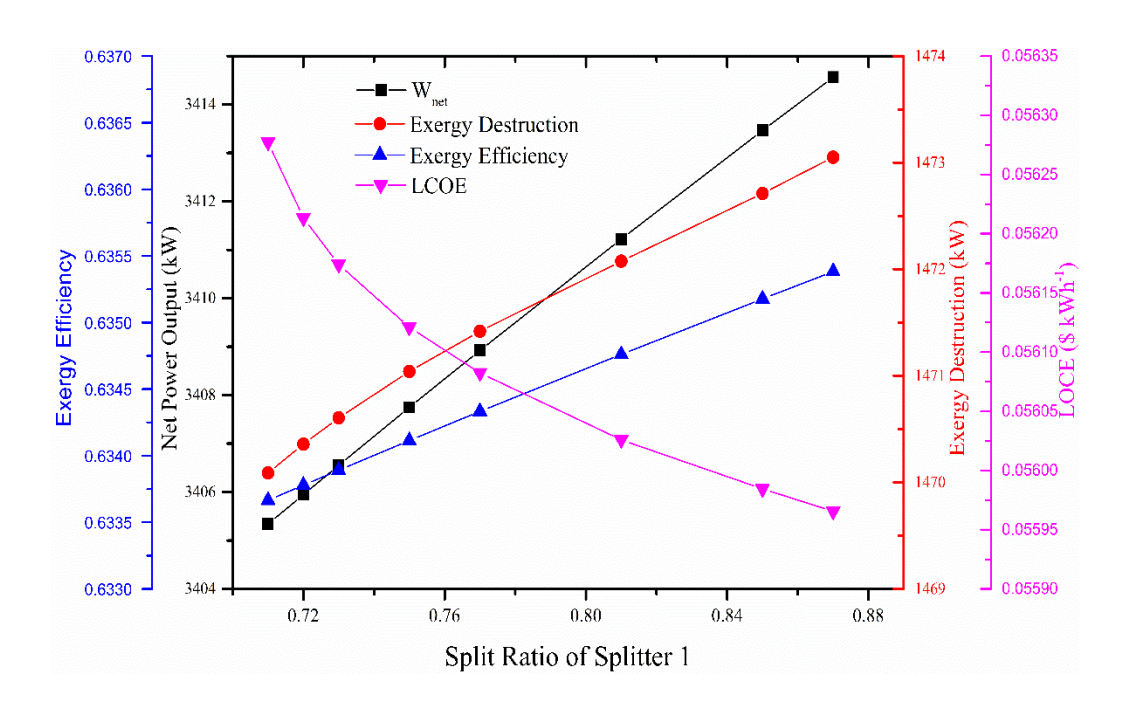


Fig. 10. Effects of the split ratio of the SCO₂BC on different parameters for the combined system.

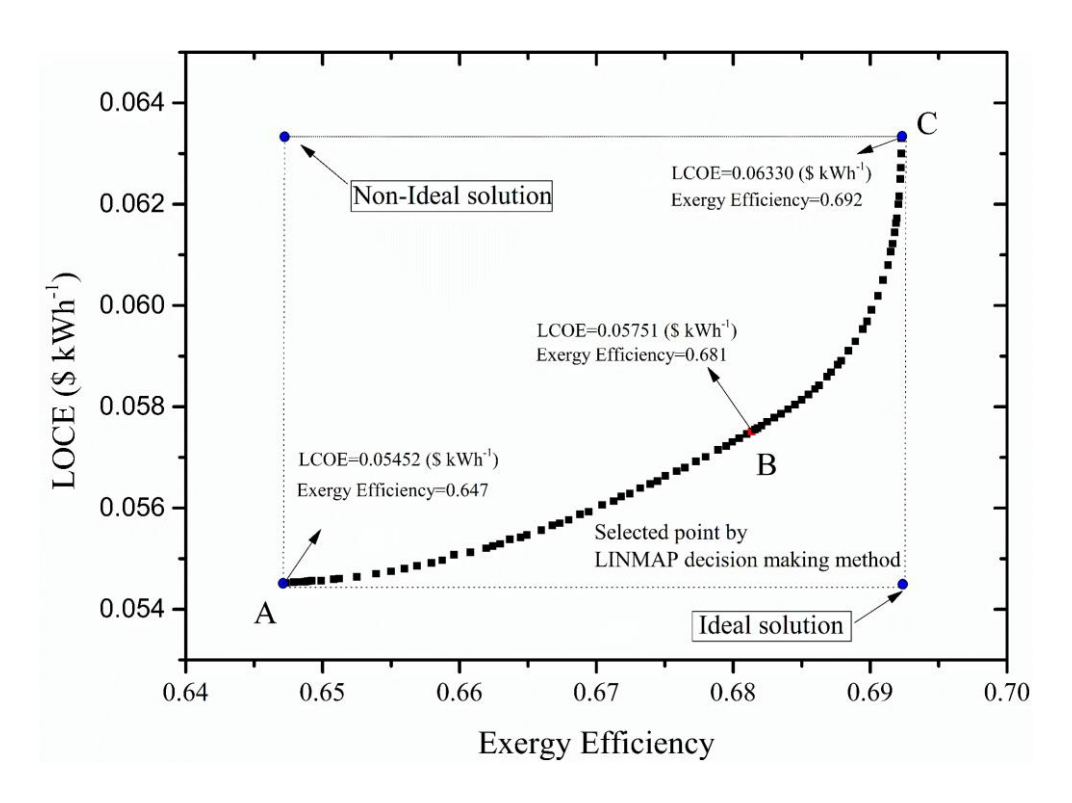


Fig. 11. Pareto frontier for integrated power system.

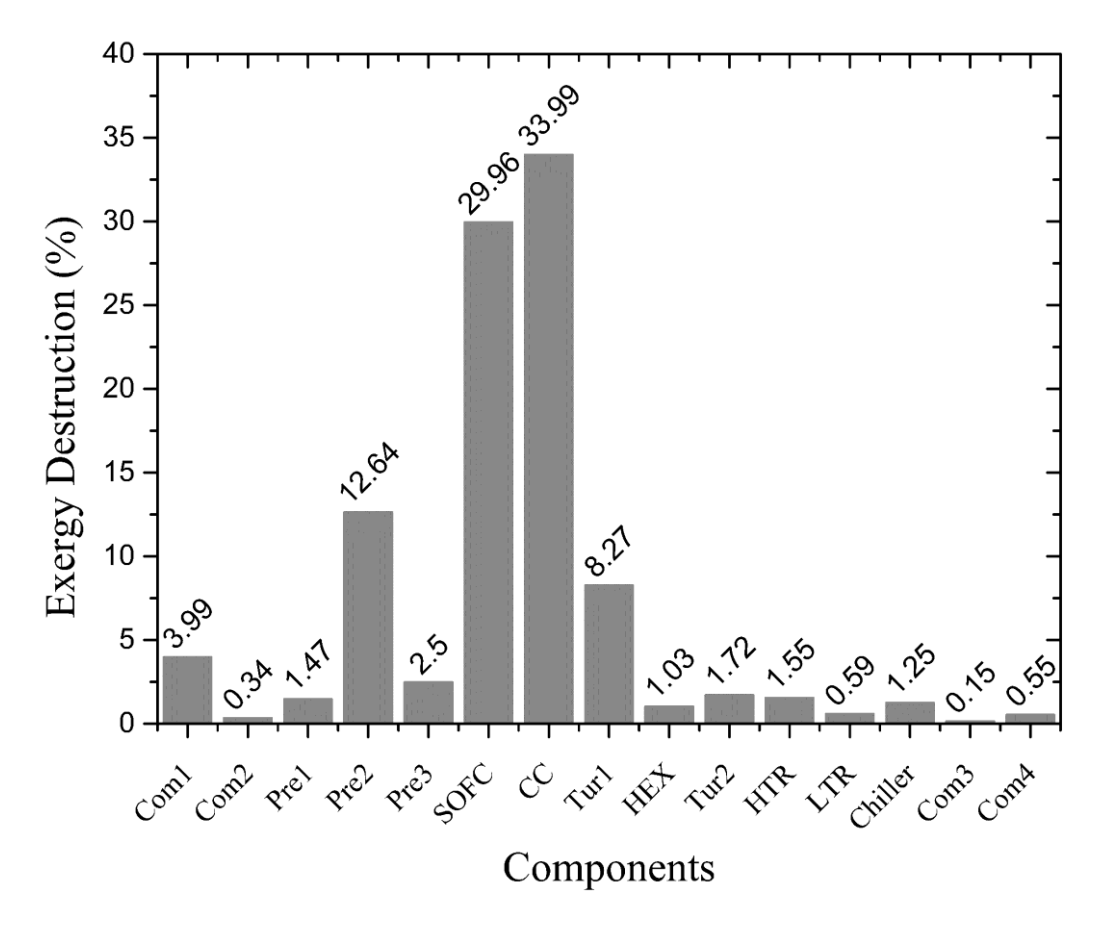


Fig. 12. The relative exergy destruction rate (%) of various components.

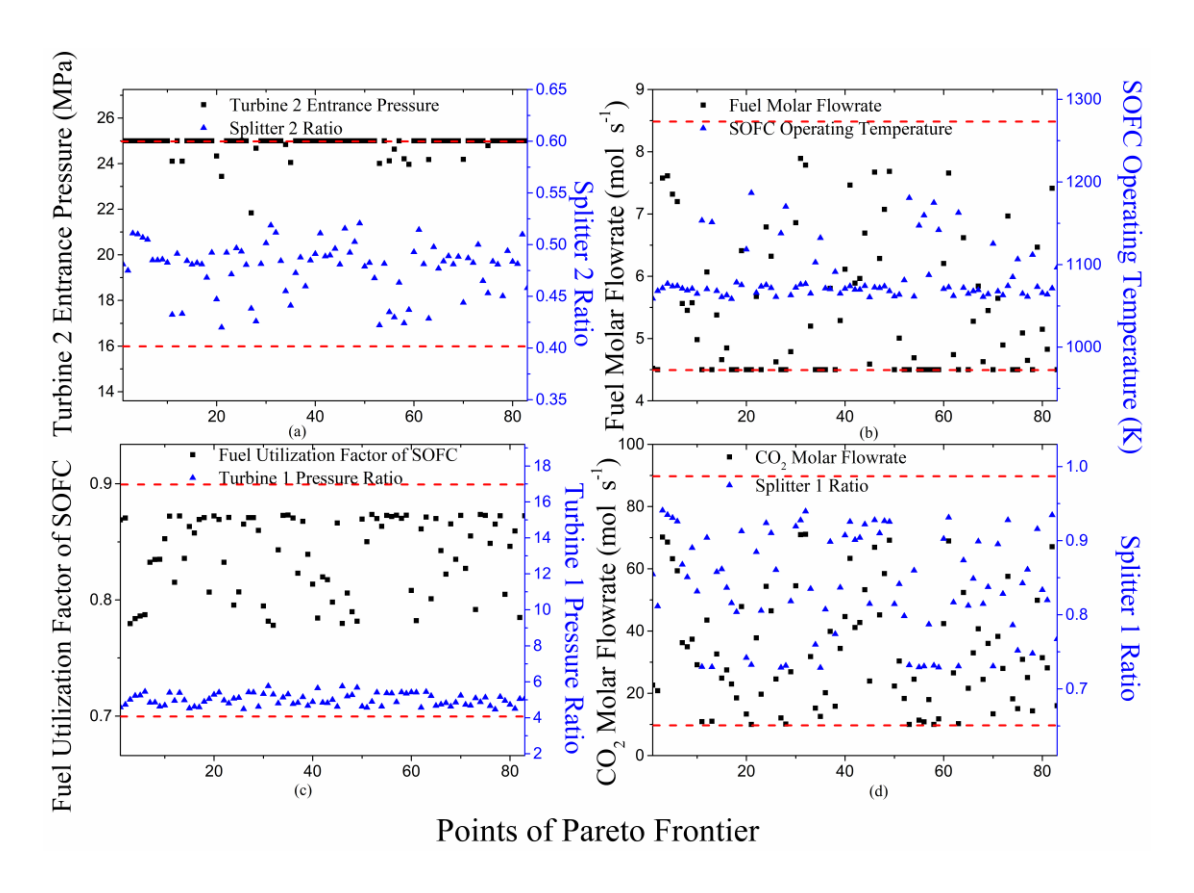


Fig. 13. Scattered distribution of (a) the turbine 2 entrance pressure and splitter 2 ratio, (b) the fuel molar flowrate and SOFC operating temperature, (c) the utilization factor of the SOFC and turbine 1 pressure ratio, (d) the CO₂ molar flowrate and splitter 1 ratio for the combined system with population in Pareto frontier.